

p75 Regulates Purkinje Cell Firing by Modulating SK Channel Activity through Rac1*

Received for publication, June 17, 2014, and in revised form, September 11, 2014. Published, JBC Papers in Press, September 24, 2014, DOI 10.1074/jbc.M114.589937

JinBin Tian^{†**}, Chhavy Tep^{§¶}, Alex Benedick[§], Nabila Saidi[§], Jae Cheon Ryu[§], Mi Lyang Kim[§], Shankar Sadasivan^{||}, John Oberdick^{||}, Richard Smeyne^{||}, Michael X. Zhu^{†**1}, and Sung Ok Yoon^{§2}

From the [§]Department of Molecular and Cellular Biochemistry, the [¶]Biochemistry Program, and the [†]Department of Neuroscience, Ohio State University, Columbus, Ohio 43210, the ^{||}Department of Developmental Neurobiology, St. Jude Children's Research Hospital, Memphis, Tennessee 38105, and the ^{**}Department of Integrative Biology and Pharmacology, University of Texas Health Science Center at Houston, Houston, Texas 77030

Background: The role of p75 in Purkinje cells of the adult cerebellum has remained obscure.

Results: In the absence of p75, RacGTP levels from the cerebellum were reduced, and the mean firing frequency for all phasic firing Purkinje cells was increased.

Conclusion: p75 regulates Purkinje cell firing by activating Rac1, thereby targeting SK channel function.

Significance: p75 signaling contributes to normal function of Purkinje cell firing.

p75 is expressed among Purkinje cells in the adult cerebellum, but its function has remained obscure. Here we report that p75 is involved in maintaining the frequency and regularity of spontaneous firing of Purkinje cells. The overall spontaneous firing activity of Purkinje cells was increased in p75^{-/-} mice during the phasic firing period due to a longer firing period and accompanying reduction in silence period than in the wild type. We attribute these effects to a reduction in small conductance Ca²⁺-activated potassium (SK) channel activity in Purkinje cells from p75^{-/-} mice compared with the wild type littermates. The mechanism by which p75 regulates SK channel activity appears to involve its ability to activate Rac1. In organotypic cultures of cerebellar slices, brain-derived neurotrophic factor increased RacGTP levels by activating p75 but not TrkB. These results correlate with a reduction in RacGTP levels in synaptosome fractions from the p75^{-/-} cerebellum, but not in that from the cortex of the same animals, compared with wild type littermates. More importantly, we demonstrate that Rac1 modulates SK channel activity and firing patterns of Purkinje cells. Along with the finding that spine density was reduced in p75^{-/-} cerebellum, these data suggest that p75 plays a role in maintaining normalcy of Purkinje cell firing in the cerebellum in part by activating Rac1 in synaptic compartments and modulating SK channels.

p75 is widely expressed during brain development, but in the adult brain, its expression is most notable in cholinergic neurons of the septum and Purkinje cells of the cerebellum.

* This work was supported, in whole or in part, by National Institutes of Health Grants NS039472 (to S. O. Y.), GM092759 (to M. X. Z.), and P30NS045758 (to the Ohio State Neuroscience Center Core).

¹ To whom correspondence should be addressed: Dept. of Integrative Biology and Pharmacology, University of Texas Health Science Center at Houston, 6431 Fannin St., Houston, TX 77030. Tel.: 713-500-7505; E-mail: michael.x.zhu@uth.tmc.edu.

² To whom correspondence should be addressed: Dept. of Molecular and Cellular Biochemistry, Ohio State University, 1060 Carmack Rd., Columbus, OH 43210. Tel.: 614-292-8542; E-mail: sung.yoon@osumc.edu.

Although the role of p75 in septal cholinergic neurons appears to be related to cell survival and degeneration (1), its role in Purkinje cells has remained largely undetermined. It has been reported, based on analysis of compound BDNF^{+/-}:p75^{-/-} mice, that p75 plays a role in dendritic development of Purkinje cells and cerebellar fissure formation, both in BDNF³-dependent and -independent manners (2). However, neither the functional consequences of such structural changes nor the mechanisms by which p75 elicits such changes are known.

We have previously reported that p75 activates Rac1 in response to neurotrophins in oligodendrocytes and Schwann cells (3, 4). As one of the small GTPases, Rac1 plays a central role in spine formation during development and in the adult, thereby regulating synaptic activity in a wide variety of neurons (5). As such, regulating its activity via its guanidine nucleotide exchange factors (6–8) and RacGTPase-activating proteins (9–11) was also known to affect not only spine morphology but also synaptic function. Interestingly, the effect of RacGTP on synaptic function is not merely a consequence of spine morphology regulation. Rac1 signaling has been shown to affect ion channels, such as Kir2.1 (12), GABA_A receptors (13), voltage-gated Ca²⁺ channels (VGCCs) (14), and GIRK channels (15) in the nervous system. These were thought to occur either through the effect of Rac1 on actin cytoskeleton (13) or its action on promoting the synthesis of phosphatidylinositol 4,5-bisphosphate (15). Conversely, RacGTP levels are regulated by neuronal activity (16, 17), including the activation of NMDA receptors (7), which orchestrates with EphB receptors to regulate Rac1 function and thereby spine morphogenesis through actin remodeling (8, 18). Therefore, Rac1 can modulate neuronal activities at multiple levels during development and plasticity, including acute effects through ion channel regulation and

³ The abbreviations used are: BDNF, brain-derived neurotrophic factor; GIRK, G-protein coupled inwardly rectifying potassium channel; VGCC, voltage-gated Ca²⁺ channel; p-PAK, phospho-PAK; aCSF, artificial cerebrospinal fluid; TEA, tetraethylammonium; AP, action potential; AHP, afterhyperpolarization; TTX, tetrodotoxin; Pn, postnatal day n; SK, small conductance Ca²⁺-activated K⁺; BK, large conductance Ca²⁺-activated K⁺.

long term consequences resulting from structural changes of dendritic arbors and spines. Indeed, dysregulation of Rac1 has been implicated in several mental disorders, such as schizophrenia (19) and fragile X syndrome (20).

Here, we report that p75 also activates Rac1 in synaptic compartments of cerebellar Purkinje cells, and this activation plays a role in maintaining normal firing regularity of Purkinje neurons through, at least in part, regulation of small conductance Ca^{2+} -activated K^{+} (SK) channels.

EXPERIMENTAL PROCEDURES

Antibodies—Phospho-PAK, PAK, and PSD95 antibodies were from Cell Signaling; Rac1, Cdc42, and tubulin antibodies were from Santa Cruz Biotechnology, Inc.; SK2 antibody was from Alomone Labs; and anti-mouse calbindin was from Swant.

Mouse Breeding—The p75 knock-out mice that carried the mutation in exon 3 of the p75 gene (21) and the wild type mice were obtained from heterozygote mating as littermates. The mice were back-crossed to C57/BL6 for 10 generations to make them congenic. The genotype was determined by PCR analyses of tail DNA according to Bentley and Lee (22).

Synaptosome Fractionation—The cerebellum and cerebral cortex were homogenized with Dounce homogenizers in 0.32 M sucrose and 4 mM HEPES plus 10 mM NaF, 10 $\mu\text{g}/\text{ml}$ aprotinin, 10 $\mu\text{g}/\text{ml}$ leupeptin, 1 mM vanadate, and 1 mM phenylmethylsulfonyl fluoride (PMSF). Postnuclear supernatants were centrifuged at $14,000 \times g$ for 10 min to collect the pellet, which was subsequently resuspended in the homogenization buffer and overlaid on top of a sucrose step gradient (0.8, 1, and 1.2 M). The gradient was centrifuged at $82,500 \times g$ for 2 h. The resulting fraction that was overlaid onto the interface between 1 and 1.2 M sucrose was collected and overlaid onto 0.8 M sucrose solution and centrifuged at $230,000 \times g$ for 15 min. The pellet contained both presynaptic and postsynaptic membranes, or synaptosomes.

RacGTP Assay—The synaptosome pellet was resuspended in a lysis buffer containing 25 mM HEPES (pH 7.5), 150 mM NaCl, 10 mM MgCl_2 , 1 mM EDTA, 10% glycerol, 1% Nonidet P-40, 0.25% sodium deoxycholate, 1 mM sodium orthovanadate, 25 mM NaF, 10 $\mu\text{g}/\text{ml}$ leupeptin, 10 $\mu\text{g}/\text{ml}$ aprotinin, and 2 mM PMSF. The lysates were subjected to RacGTP assays using pull-down methods as described (3).

Immunohistochemistry—Brains were sectioned at 30 μm in a sagittal or coronal plane using a cryostat and used for immunohistochemistry as described (4). For p-PAK staining, tissues were subjected to antigen retrieval at 50 °C for 50 min in 10 mM Tris-HCl (pH 9.0). The images were obtained using a Leica confocal microscope (model TCS SL) at the identical setting for wild type and p75 knock-out sections.

Organotypic Cerebellar Slices—Freshly dissected brains were cut at 200 μm on the sagittal plane at 4 °C using a vibratome (Leica), and cerebellar slices that contained all 10 lobules were placed inside a Millicell on the sagittal orientation as described (24). BDNF was added to the underlying media at 50 ng/ml, incubated for 10 min at 37 °C, and processed for protein extraction.

Preparation of Cerebellar Slices for Electrophysiological Recordings—Mice (postnatal days 15–25) were anesthetized with halothane and sacrificed by decapitation. Sagittal slices of 300- μm thickness were prepared from the vermis of the cerebellum with a vibratome (World Precision Instruments) in ice-cold, oxygenated artificial cerebrospinal fluid (aCSF): 125 mM NaCl, 26 mM NaHCO_3 , 1.25 mM NaH_2PO_4 , 2.5 mM KCl, 1 mM MgCl_2 , 2 mM CaCl_2 , and 10 mM glucose bubbled with 5% CO_2 and 95% O_2 (pH 7.4). Slices were recovered at 35 °C for 1 h and then maintained at room temperature (22–24 °C) in the aCSF until use.

Extracellular Recording—Littermate pairs of the wild type and p75^{-/-} mice were used. The recordings from each pair of littermates were performed either on the same day or on two consecutive days under the same experimental conditions. From each animal, 20–40 Purkinje cells from the apex of the lobule VI of the cerebellum were randomly recorded. Prior to recording, the cerebellar slice was mounted in a chamber on the stage of a Nikon E600-FN upright microscope and continuously perfused (2 ml/min) with a modified aCSF (*i.e.* aCSF supplemented with 5 mM kynurenic acid (a broad spectrum ionotropic glutamate receptor antagonist) and 100 μM picrotoxin (a GABA_A receptor blocker)). The solution was heated to 33–35 °C with an SC-20 in-line solution heater (Harvard Apparatus). The Rac1 inhibitor, NSC23766 (Calbiochem), was diluted in the modified aCSF to 100 μM and applied through whole-chamber perfusion. Extracellular field potentials were recorded using glass electrodes with a tip size of 0.5–1 μm filled with aCSF without the synaptic blockers. The pipette tip was positioned near the initial axon segment of the Purkinje cell soma. Action potentials appeared as fast negative deflections of 100–1000 μV . Only clearly isolated single cell signals were chosen for recording and subsequent analysis. Signals were preamplified and filtered (at 3 kHz) by NPI EXT-10C and LPBF-01GX amplifier/filter modules before being digitized and sampled (at 10 kHz) by the built-in AD/DA converter of an EPC10 amplifier (HEKA Electronics Inc.). Data were analyzed using the Spike2 program (Cambridge Electronic Design).

Whole-cell Current Clamp Recording—Recording pipettes were pulled from micropipette glass (A-M Systems, Inc., Carlsborg, WA) to 3–5 M Ω and filled with an intracellular solution containing 122 mM potassium gluconate, 9 mM NaCl, 1.8 mM MgCl_2 , 0.9 mM EGTA, 9 mM HEPES, 14 mM Tris-creatine phosphate, 4 mM Mg-ATP, and 0.3 mM Tris-GTP (pH 7.2) and placed in the modified aCSF. When needed, NSC23766 was diluted in the intracellular solution and applied into the cytoplasm of Purkinje cells through dialysis from the recording pipette. Purkinje cells in lobule VI of mouse cerebellar slices were selected for whole-cell recording using an EPC10 amplifier and the PatchMaster version 2.2.0 software while the slice was continuously perfused with the modified aCSF at 33 °C. Tight (G Ω) seal and high quality break-in were made using the ez-gSEAL pressure controller (NeoBiosystems, Inc., San Jose, CA). As soon as the whole-cell configuration was established, fast and slow capacitances were canceled, and the holding potential was set to -70 mV. Spontaneous firing was recorded after switching to current clamp mode and setting the current

p75 Regulates SK Channels in Purkinje Cells

injection value to 0. Voltage signals were sampled at 20 kHz using a gap-free recording protocol.

Acute Isolation of Purkinje Cells—Cerebellar Purkinje neurons were isolated as described (69). In brief, the vermal layer of the cerebellum from the wild type or p75^{-/-} mice (P13–P18) was removed and minced in an ice-cold, oxygenated dissociation solution containing 82 mM Na₂SO₄, 30 mM K₂SO₄, 5 mM MgCl₂, 10 mM HEPES, 10 mM glucose, and 0.001% phenol red (pH 7.4). The minced tissue was subsequently incubated in the dissociation solution with 3 mg/ml protease XXIII (pH 7.4; Sigma) at 35 °C for 7 min while oxygen was blown over the surface of the solution. Subsequently, the tissue was washed in prewarmed, oxygenated dissociation solution containing 1 mg/ml bovine serum albumin and 1 mg/ml trypsin inhibitor and then maintained in Tyrode's solution containing 150 mM NaCl, 4 mM KCl, 2 mM CaCl₂, 2 mM MgCl₂, 10 mM HEPES, and 10 mM glucose at room temperature (pH 7.4) while oxygen was blown over the surface of the fluid. Occasionally, an aliquot of the tissue suspension was withdrawn and triturated with a fire-polished Pasteur pipette to liberate individual neurons. Purkinje cells were identified by their large diameter and characteristic pearlike shape. Dendrites were rarely seen, but some dendritic membrane may have been incorporated into the isolated neurons. Cells were used between 30 min and 4 h of dissociation.

Whole-cell Voltage Clamp Recording of Isolated Purkinje Cells—Acutely dissociated Purkinje cells were allowed to settle in the recording chamber for 5 min. After washing out tissue debris with Tyrode's solution, Purkinje cells with a pearlike shape and smooth surface were selected. Recording pipettes (2–4 MΩ) were filled with an intracellular solution containing 122 mM potassium gluconate, 9 mM NaCl, 1.8 mM MgCl₂, 0.9 mM EGTA, 9 mM HEPES, 14 mM Tris-creatine phosphate, 4 mM MgATP, and 0.3 mM Tris-GTP (pH 7.2). The control external solution was Tyrode's solution, which was applied to the recorded cell during the gigaseal formation. After adding 300 nM tetrodotoxin (TTX) to Tyrode's solution to block all major sodium channels, the solution was referred to as "Ca ECS". A "Co ECS" solution was made by replacing CaCl₂ in Ca ECS with 2 mM CoCl₂, which reversibly blocks calcium currents through all types of calcium channels. In order to block certain potassium channels, tetraethylammonium (TEA; 1 mM) was added to Ca ECS and Co ECS to make "CaTEA ECS" and "CoTEA ECS," respectively. Fast change of different ECS was achieved by using a pressure-driven, solenoid valve-controlled perfusion system (SmartSquirt 8, AutoMate Scientific). The open end of the perfusion probe was positioned near the cell to ensure complete coverage of the cell by the perfusate. Whole-cell recordings of isolated Purkinje cells were performed at room temperature (22–24 °C) using the EPC10 amplifier. Current signals were digitized at 10 kHz. After establishment of the whole-cell configuration, the cell was voltage-clamped at –80 mV. Fast and slow capacitances were canceled using the auto compensation function of the PatchMaster software. For isolation of potassium currents, voltage step protocols were repeated when the cell was exposed to Ca ECS, Co ECS, CaTEA ECS, and CoTEA ECS sequentially. For quantification of ionic currents of

interest, recordings from the last three ECS solutions were subtracted from their corresponding control records.

Whole-cell Voltage Clamp Recording of SK-mediated Tail Current—To evaluate SK channel activities, we adopted a voltage clamp protocol used previously to isolate SK-mediated tail currents in cerebellar Purkinje cells (25). For this study, cerebellar slices prepared from a pair of wild type and p75^{-/-} littermates were recorded on the same day. The slice was perfused with aCSF supplemented with 1 μM TTX and 1 mM TEA to block voltage-gated Na⁺ channels, most of the voltage-gated K⁺ channels, and large conductance Ca²⁺-activated K⁺ (BK) channels. Drugs (100 nM apamin or 100 μM NSC23766) were applied to the cerebellar slice through bath perfusion. Purkinje cells located in lobules V–VII were randomly picked. The patch electrode was filled with an intracellular solution containing 135 mM potassium gluconate, 10 mM KCl, 1 mM MgCl₂, 2 mM Na₂-ATP, 0.4 mM Na₃-GTP, 10 mM HEPES (pH 7.2–7.3 with KOH). Purkinje cells were held at –50 mV before stepping to potentials ranging from –10 to +30 mV every 30 s for a period of 100–300 ms to induce unclamped Ca²⁺ spike complexes. At the end of the voltage step, the membrane potential was stepped back to –50 mV to allow for the generation of Ca²⁺-activated tail currents. Using this protocol, currents evoked during the voltage step were not fully clamped due to space clamp errors. However, the voltage control after the step back to –50 mV can be well maintained (26, 27). Because individual Purkinje cells responded to the same voltage step with distinct numbers and positions of Ca²⁺ spike complexes, which could strongly affect the size and shape of the tail currents, special care was taken to maintain the constant number and position of Ca²⁺ spikes before and during the drug application. In most recordings, step parameters were adjusted to allow only one Ca²⁺ spike complex with the peak occurring right in the middle of the step (see Fig. 3A (a), region 2, inward peak). This ensured no or little overlap between currents of the Ca²⁺ spike complex and the tail current and a good consistency of all tail currents recorded from the same cell. SK currents were evaluated based on either the peak tail current amplitude (for the comparison between p75^{+/-} and p75^{-/-} neurons) or the tail current amplitude at the time when maximal inhibition by NSC23766 was achieved. Because the size of the Ca²⁺ spike may potentially affect tail current amplitude, SK tail current was normalized to the integral of the Ca²⁺ spike complex from the same recording and then used for paired comparison between p75^{+/-} and p75^{-/-} cells (for Fig. 3C (c)) and for paired comparison before and during the NSC23766 treatment for the same cell (for Fig. 6B (b)).

Electrophysiological Data Analysis—Data were processed in Microsoft Excel 2010, Origin version 8.0 (OriginLab), and Statistica version 7.1 (StatSoft) programs. Data are presented as means ± S.E. Statistical analysis was performed using Student's *t* test and analysis of variance. *p* < 0.05 was defined as statistically significant.

Electron Microscopic (EM) Analysis—Mice were perfused with 2% paraformaldehyde, 2% glutaraldehyde in 0.1 M sodium cacodylate buffer (pH 7.2) prior to dissecting the brain (*n* = 3 for each genotype). The brain was first cut in a sagittal plane, and 1 × 1-mm square areas were cut out from the lobule VI/VII.

The tissues were rinsed in 0.1 M sodium cacodylate buffer and placed in 1% osmium, 0.1 M sodium cacodylate for 1–1.5 h at room temperature. The tissues were stained en bloc for 1 h in 2% uranyl acetate and embedded in Spurr resin following dehydration procedures. Sections were cut at 80 nm using a Reichert Ultracut E ultramicrotome and collected on 300-mesh grids. Sections were stained in 2% uranyl acetate and Reynolds lead citrate before observation in an FEI Technai G2 Spirit transmission electron microscope at 60 kV (Ohio State University Campus Microscopy and Imaging Facility).

For quantification of spine head areas, the electron photomicrographs were taken at $\times 15,750$ magnification, and the spine length and spine head area were calculated using ImageJ software in a blinded manner. For statistical analyses, Student's *t* test was used.

Golgi-Cox Analysis—Freshly dissected brains were stained for Golgi analysis using the Rapid GolgiStain™ kit as directed by the manufacturer (FD Neurotechnologies Inc.) and sectioned in the sagittal plane at 200 μm . Five Purkinje neurons from each of lobes IV, V, VI, and VII of each cerebellum per set of p75^{+/+} and p75^{-/-} mice (*n* = 3) were then analyzed in a blinded manner using the NeuroLucida® 7 image analysis system (MBF Biosciences), and the spine density was determined. For each Purkinje neuron, at least five different dendritic secondary and tertiary branches were randomly selected for spine analysis at $\times 100$ magnification to obtain the number of spines per given length of the dendritic branch. For statistical analyses, Student's *t* test was used.

RESULTS

p75 Modulates Spontaneous Firing Properties of Purkinje Cells—Rodent cerebellar Purkinje cells are known to fire spontaneously in the absence of any afferent inputs at a relatively constant rate (tonic firing) or intermittently with pauses of variable lengths that separate the firing periods (phasic firing). During phasic firing, there can also be a short duration of bursting, which typically precedes long pauses or silence periods, giving rise to the so-called trimodal firing pattern of Purkinje neurons (28, 29). To test whether p75 modulates this intrinsic spontaneous firing activity of Purkinje cells, we performed extracellular recordings on Purkinje neurons that were randomly selected from the apex of lobule VI in acute cerebellar slices from P18–P25 mice in the presence of kynurenic acid (5 mM) and picrotoxin (100 μM) to block fast synaptic transmission mediated by AMPA and GABA_A receptors, respectively. We found that the mean firing frequency over a 5-min period of all p75^{-/-} neurons was increased by 15% when they were compared as littermate pairs with the wild type (Fig. 1A). When tonic firing cells were separated from phasic firing ones, on the other hand, the increase was only found in phasic firing cells and not tonic firing ones (Fig. 1, B and C); whereas it was similar for tonic firing cells between p75^{+/+} and p75^{-/-} mice, the mean firing frequency for all phasic firing Purkinje cells was increased by 41% in p75^{-/-} mice. For this analysis, the phasic firing cells included typical trimodal firing cells (28, 29) and atypical ones that either lacked the bursting phase or showed large variations in firing rates with no obvious patterns. The proportions of phasic firing Purkinje neurons were 48 and 40% in the wild type and p75^{-/-}

mice, respectively. These results suggest that p75 plays a role in modulating intrinsic, spontaneous firing of cerebellar Purkinje neurons.

To understand the underlying cause(s) for the increased mean firing frequency in p75^{-/-} Purkinje neurons, we analyzed the interspike intervals during tonic periods or interburst intervals during bursting periods, but no significant differences were found (data not shown). Instead, we found that the overall silence periods between the firing phases were shorter and less frequent in Purkinje neurons from p75^{-/-} mice than that from the wild type (Fig. 1D). For quantification, we plotted the sum of all intervals that were longer than 1 s during the 5-min recording for each cell. These intervals only include the long silence between firing periods, because typical interspike intervals are <50 ms, and interburst intervals are <250 ms. The mean silence duration was reduced by 27% in p75^{-/-} cells compared with wild type cells (Fig. 1E). Conversely, the total firing periods (tonic plus bursting periods) were longer in p75^{-/-} than in wild type cells, with the ratio of firing to silencing 71% higher in p75^{-/-} than in wild type cells (Fig. 1F). These data suggest that the loss of p75 rendered Purkinje cells free to fire for longer periods of time, with a reduced probability of going into the silence phase.

It is possible that the increase in firing period was due to the fact that p75^{-/-} cells cannot maintain the silence phase, rather than firing longer. Our data suggest that this is unlikely, because plotting distributions of all intervals that are longer than 1 s did not reveal any difference between the two genotypes (Fig. 1G). The number of silence periods within the same 5-min recording, on the other hand, was significantly reduced in p75^{-/-} compared with p75^{+/+} neurons, especially for intervals that are longer than 4 s (Fig. 1H). These analyses are consistent with an overall increase in the firing duration in p75^{-/-} cells and explain the calculated higher mean firing frequency among phasic firing p75^{-/-} cells.

p75 Facilitates Ca²⁺-activated TEA-insensitive K⁺ Channels in Purkinje Cells—It is possible that the difference between p75^{+/+} and p75^{-/-} Purkinje neurons is due to changes in action potential (AP) waveforms. We thus analyzed AP threshold, AP amplitude, AP rise time (10–90%), AP decay time (90–37%), afterhyperpolarization (AHP) peak amplitude, and time from AP peak to 90% maximal AHP but did not find any difference between p75^{-/-} and p75^{+/+} neurons (data not shown). These results suggest that AP characteristics do not differ between the two genotypes.

Both BK and SK channels have been shown to modulate Purkinje cell firing, with BK strongly affecting spike timing of burst firing and SK contributing more to burst termination (29–31). We thus hypothesized that one of the mechanisms by which p75 regulates firing frequency in Purkinje cells may involve Ca²⁺-activated K⁺ channels. The hypothesis was tested by measuring Ca²⁺-dependent, TEA-insensitive K⁺ currents using whole-cell voltage clamp recordings of acutely dissociated Purkinje cells from p75^{+/+} and p75^{-/-} mice. In these assays, TTX (300 nM) was included in all recordings to block voltage-gated Na⁺ channels. We used TEA (1 mM) to reveal the contribution of TEA-sensitive K⁺ channels and used cobalt chloride (CoCl₂; 2 mM) in place of CaCl₂, to determine the

p75 Regulates SK Channels in Purkinje Cells

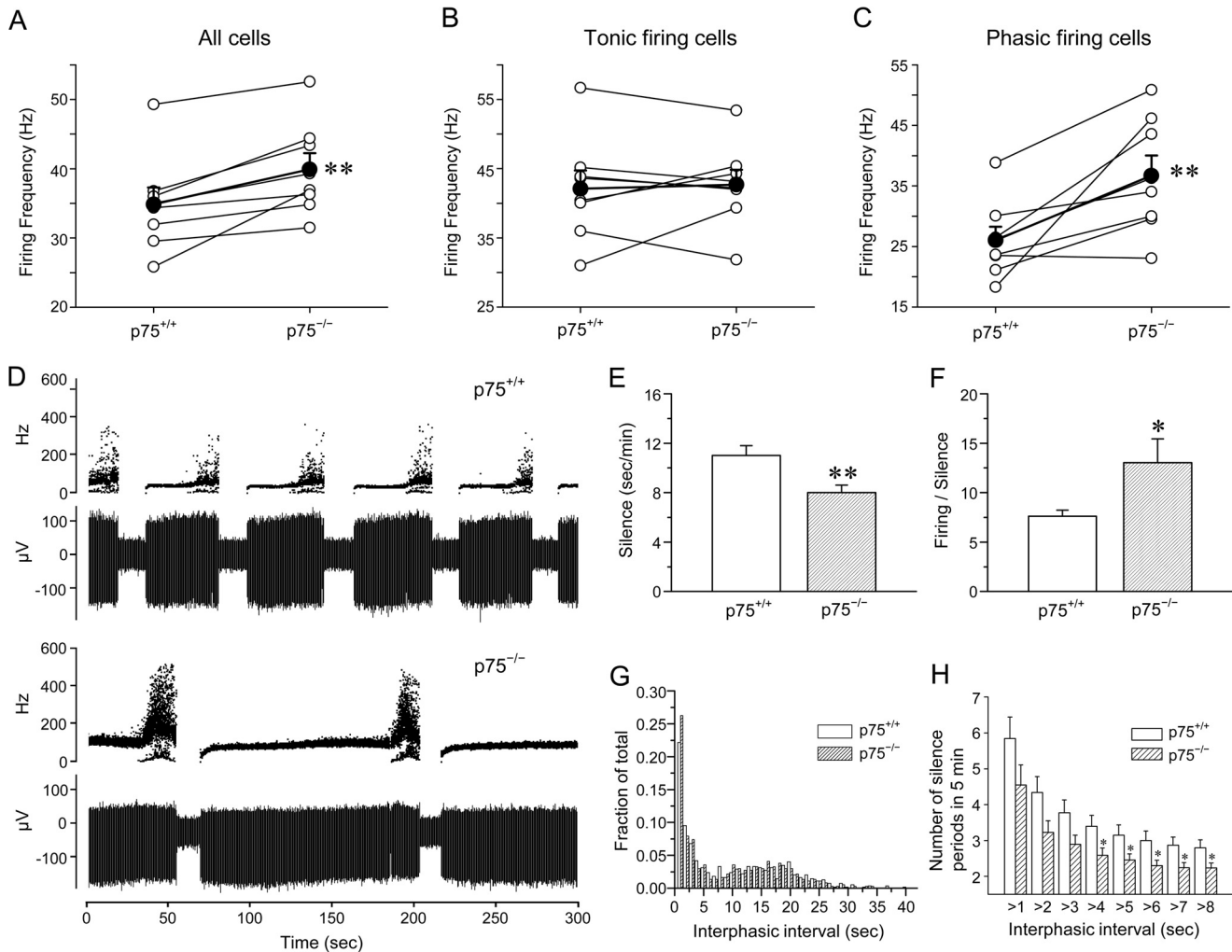


FIGURE 1. p75 influences spontaneous firing properties of Purkinje cells by extending the firing period. A–C, mean firing frequencies were increased in p75^{-/-} compared with p75^{+/+} Purkinje cells, especially during phasic firing mode. The data represent pair-wise comparisons of extracellular recordings in cerebellar slices from p75^{+/+} and p75^{-/-} littermates, which were recorded on the same day or on two consecutive days. The *open circles* represent the mean firing frequency of all recorded cells from each mouse, and the average value of seven pairs is shown by the *filled circles*. **, $p < 0.01$ by paired Student's *t* test. A, mean firing frequencies of all recorded cells were increased by 15% in p75^{-/-} Purkinje cells compared with p75^{+/+} Purkinje cells. B, mean firing frequencies were similar between p75^{-/-} and p75^{+/+} Purkinje cells among tonic firing cells. C, mean firing frequencies were increased by 41% in p75^{-/-} compared with p75^{+/+} phasic firing Purkinje cells. D, overall silence periods were reduced in p75^{-/-} Purkinje neurons compared with the wild type. Representative traces of a phasic firing cell from a p75^{+/+} or a p75^{-/-} mouse are shown. The *top traces* illustrate instantaneous firing frequency, and the *bottom traces* show the field potential changes during the 5-min recording periods. The sharp increases in the instantaneous firing frequencies and broader distributions of such frequencies at the end of the firing phase represent the burst firing period, which typically precedes the silence phase. E, quantification of the total silence period per unit time during phasic firing indicates that there is a 27% reduction in p75^{-/-} compared with p75^{+/+} Purkinje cells. F, quantification of the firing/silence ratio for all phasic firing cells recorded indicates that there is a 71% increase in p75^{-/-} compared with p75^{+/+} Purkinje cells. The data in E and F are means \pm S.E. (error bars) for 101 p75^{+/+} and 86 p75^{-/-} neurons. *, $p < 0.05$; **, $p < 0.01$ by Student's *t* test. G, interphasic intervals that are longer than 1 s are similarly distributed between p75^{+/+} and p75^{-/-} neurons. H, the number of silence periods was reduced in p75^{-/-} compared with p75^{+/+} neurons, especially for interphasic intervals that are longer than 4 s. Shown are means \pm S.E. for interphasic intervals that are longer than the specified durations indicated on the x axis. *, $p < 0.05$ by Student's *t* test.

contribution of VGCCs and consequently Ca²⁺-activated K⁺ channels. Using the voltage clamp step protocol, as shown in Fig. 2A, currents were recorded in the absence and presence of 1 mM TEA and with the extracellular bath solution containing either 2 mM CaCl₂ (Fig. 2B) or 2 mM CoCl₂ (Fig. 2C). Ca²⁺-dependent and TEA insensitive K⁺ currents were obtained by subtracting the TEA-insensitive currents recorded in the presence of CoCl₂ from that recorded in the presence of CaCl₂ (Fig. 2D). The maximum outward current obtained at each holding potential was normalized to that at 10 mV in the presence of 2 mM CaCl₂ and absence of TEA.

As shown by the current-voltage (*I-V*) relationship plots in Fig. 2, E–G, whereas the TEA sensitive current did not show

significant difference between wild type and p75^{-/-} cells regardless of Ca²⁺ or Co²⁺ in the bath, the differential currents between -30 and 10 mV, representing Ca²⁺ dependent and TEA-insensitive K⁺ channels, were reduced by 23% in the p75^{-/-} Purkinje cells as compared with the wild type (Fig. 2G). Ca²⁺-dependent K⁺ channels that are insensitive to 1 mM TEA include SK channels (32, 33). In cerebellar Purkinje cells, SK channels were reported to play a major role in regulating firing frequency and cycle duration of the trimodal firing pattern primarily in dendrites (29, 34). Our data therefore suggest that p75 may play a role in maintaining normal levels of SK channel activities, thereby regulating firing properties of Purkinje cells.

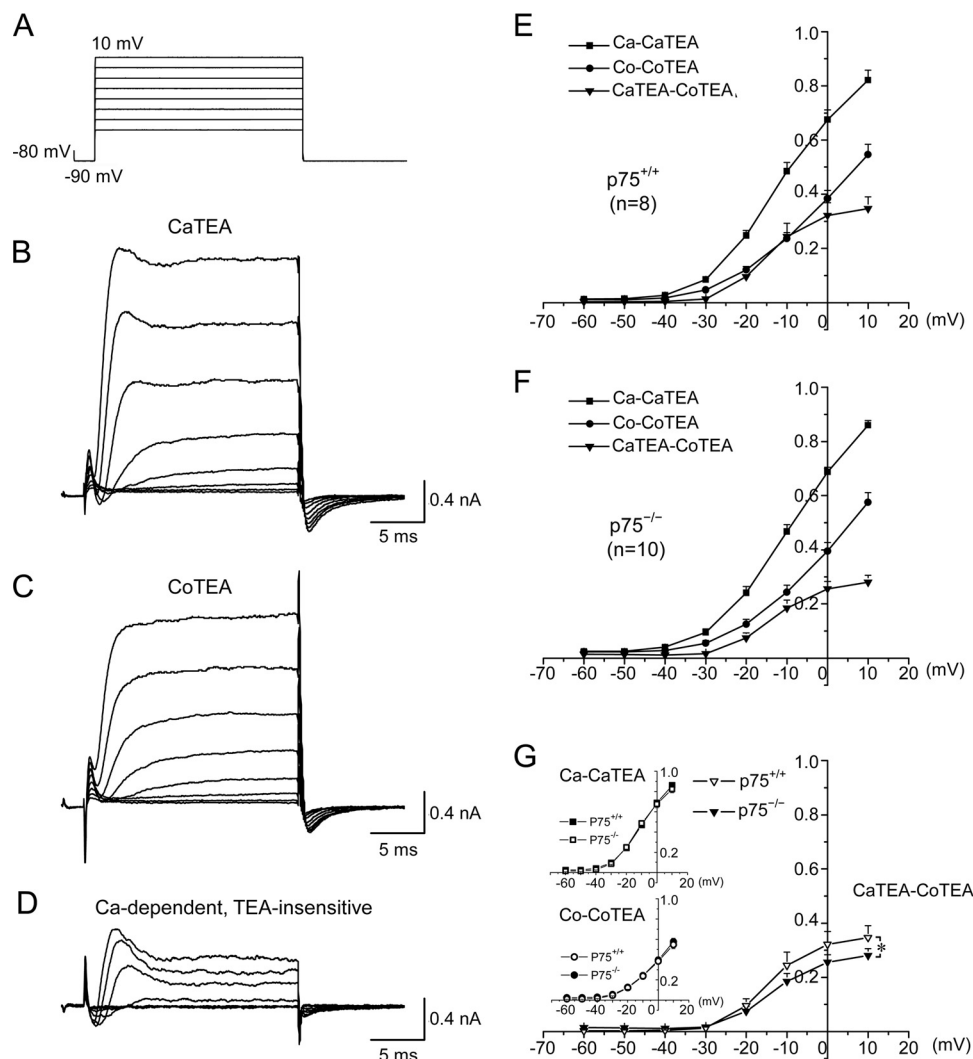


FIGURE 2. p75 facilitates Ca²⁺-dependent, TEA-insensitive K⁺ current in Purkinje cells. *A*, voltage steps used for whole-cell voltage clamp recording of acutely dissociated Purkinje cells. *B* and *C*, representative traces from a wild type neuron bathed in the CaTEA solution containing 2 mM Ca²⁺, 300 nM TTX, and 1 mM TEA (*B*) or bathed in the CoTEA solution containing 2 mM Co²⁺, 300 nM TTX, and 1 mM TEA (*C*). *D*, subtracted traces of *B* and *C*, representing the activity of Ca²⁺-dependent but TEA-insensitive K⁺ channels. The inward currents observed at the start of the recording represent calcium channel activities. *E* and *F*, average current-voltage (*I*-*V*) curves under the conditions depicted in *B*-*D* for p75^{+/+} (*E*) and p75^{-/-} (*F*) Purkinje neurons. *G*, comparison of *I*-*V* curves between Purkinje cells from p75^{+/+} and p75^{-/-} mice revealed that Ca²⁺-dependent and TEA-insensitive K⁺ currents were reduced by 23% in p75^{-/-} Purkinje cells as compared with the wild type. Note that in *E*-*G*, current amplitudes were normalized to the maximal value obtained in the absence of TEA but in the presence of 2 mM Ca²⁺; thus, the y axis in *E*-*G* indicates normalized currents. Significant differences (analysis of variance; *p* < 0.05) are found for the Ca²⁺-dependent TEA-insensitive K⁺ currents (CaTEA-CoTEA) between -30 and 10 mV. Error bars, S.E.

p75 Regulates SK Channel Activities in Purkinje Cells—To determine whether SK channel activity is down-regulated in p75^{-/-} Purkinje neurons, we recorded SK-mediated tail currents in Purkinje cells from cerebellar slices by whole-cell voltage clamping. SK-mediated tail currents were elicited by a transient Ca²⁺ influx mediated by VGCCs in response to depolarizing voltage steps. As demonstrated previously in rat Purkinje cells (25), when voltage-gated Na⁺ channels and most voltage-gated K⁺ channels (including BK channels) were blocked by TTX and 1 mM TEA, respectively, the outward tail current measured immediately after returning the voltage to -50 mV was mainly attributable to SK channels.

Using this protocol, we first tested to what extent the tail current following voltage steps could be blocked by the specific SK channel blocker, apamin, in wild type mouse Purkinje cells. As shown in Fig. 3*A* (*a*), a Ca²⁺ spike complex (inward current)

evoked by a 300-ms voltage step from -50 mV to 0 mV (Fig. 3*A* (*a*), region 2) was immediately followed by an outward tail current (Fig. 3*A* (*a*), region 3). Bath perfusion of 100 nM apamin almost completely eliminated the tail current (Fig. 3*A* (*b*), gray trace) without affecting the Ca²⁺ spikes (Fig. 3*A* (*b*), inset), confirming that under our experimental conditions, the tail currents obtained in mouse cerebellar Purkinje cells were indeed mediated by SK channels. Next, to compare SK currents in Purkinje neurons from p75^{+/+} and p75^{-/-} cerebellar slices, we applied a series of voltage steps from -40 to +30 mV before returning the holding potential to -50 mV (Fig. 3*B* (*a*)). The SK channel-mediated tail currents were reduced in p75^{-/-} Purkinje cells by ~21% compared with that in p75^{+/+} Purkinje cells at all step potentials tested, with the maximal reduction observed at -30 mV (Fig. 3*B* (*b*) for representative traces; Fig. 3*C* (*a*) for summary; *n* = 17 for p75^{+/+}, *n* = 23 for p75^{-/-}). The

p75 Regulates SK Channels in Purkinje Cells

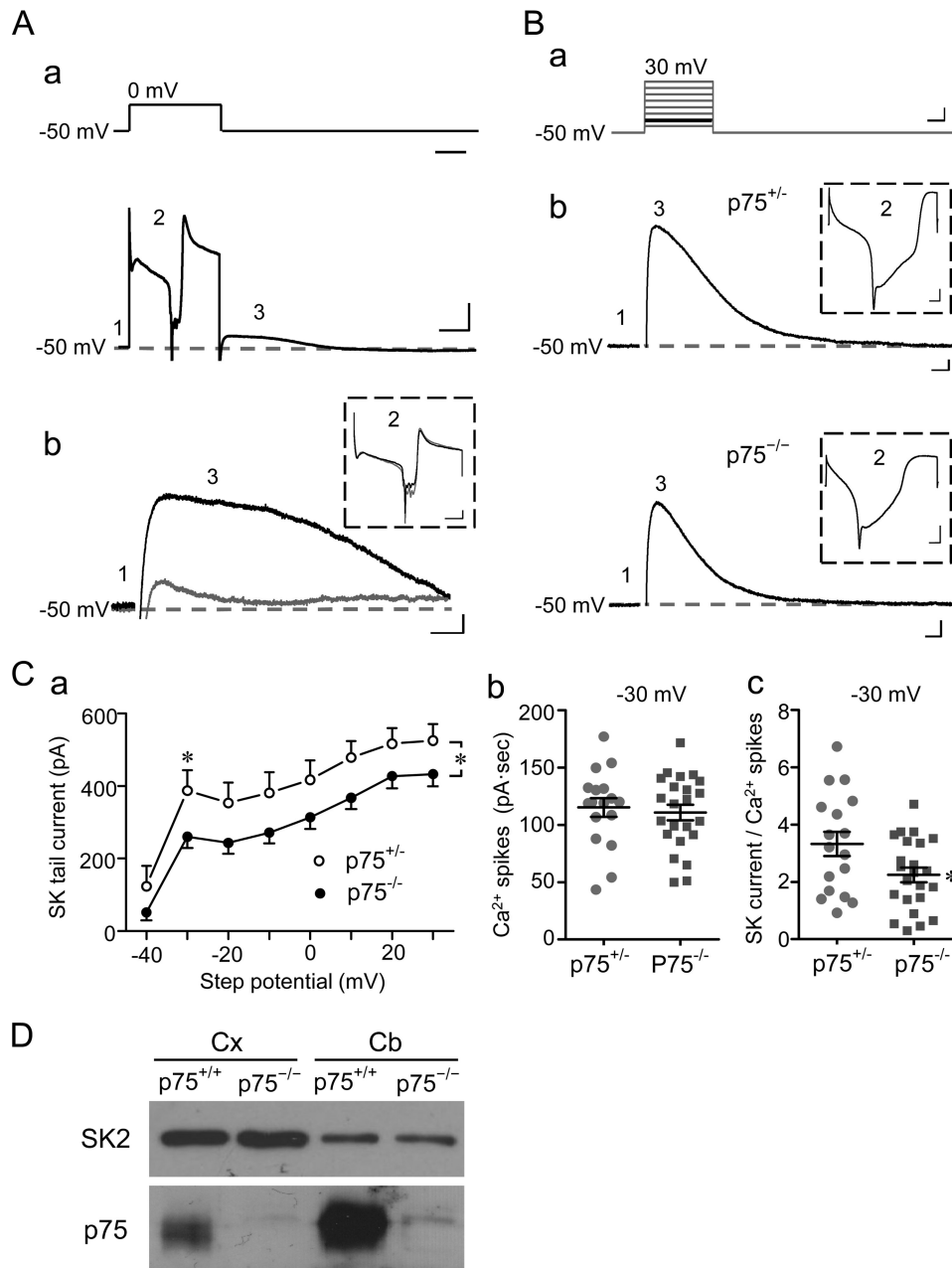


FIGURE 3. p75 regulates SK channel activity in Purkinje cells. *A (a)*, voltage step protocol used to record SK-mediated tail currents from Purkinje neurons in cerebellar slices (*top*) and a representative current trace (*bottom*) with the three regions (*numbered 1–3*) indicated. *Region 1* represents the basal current when the cell was voltage-clamped at -50 mV; *region 2* represents the current response to the voltage step, showing development and inactivation of an inward Ca^{2+} current complex; *region 3* represents the outward tail current. *A (b)*, representative traces of tail currents (*region 3*) obtained before (*black*) and during (*gray*) bath application of 100 nM apamin for the same WT Purkinje neuron. The Ca^{2+} spike complex (*region 2*) from the same record is shown in the *inset* with different scales. Scale bars, 100 ms (*A (a), top*); 100 ms, 500 pA (*A (a), bottom*); 30 ms, 30 pA (*A (b)*); and 50 ms, 300 pA (*A (b), inset*). *B (a)*, voltage step protocol used for comparing SK-mediated tail currents between $\text{p75}^{+/-}$ and $\text{p75}^{-/-}$ Purkinje neurons in cerebellar slices. The cell was held at -50 mV for 50 ms before stepping to potentials between -40 mV and $+30$ mV in eight steps (10 mV/step, 100 -ms duration, 30 -s intervals). *B (b)*, representative traces of SK-mediated tail currents from $\text{p75}^{+/-}$ and $\text{p75}^{-/-}$ Purkinje cells evoked by the voltage step to -30 mV (highlighted in *black* in *B (a)*). Scale bars, 25 ms, 20 mV (*B (a)*), 25 ms, 50 pA (*B (b)*), and 10 ms, 500 pA (*B (b), inset*). For all representative traces, the *dashed gray lines* indicate basal current levels. *C (a)*, I-V relationship of SK-mediated tail currents for $\text{p75}^{+/-}$ ($n = 17$) and $\text{p75}^{-/-}$ ($n = 23$) Purkinje cells. Peak tail currents were plotted against step potentials. *, $p < 0.05$, between $\text{p75}^{+/-}$ and $\text{p75}^{-/-}$ (two-way analysis of variance followed by LSD post hoc tests). *C (b)*, integral current of Ca^{2+} spike complex elicited by a voltage step (-50 to -30 mV) for individual neurons. Lines, mean \pm S.E. (error bars). No significance was found between $\text{p75}^{+/-}$ and $\text{p75}^{-/-}$ neurons (Student's *t* test, $p = 0.57$). *C (c)*, SK tail current normalized to the integral current of Ca^{2+} spike complex of the same recording of individual neurons. Lines, mean \pm S.E. *, $p = 0.03$ between $\text{p75}^{+/-}$ and $\text{p75}^{-/-}$ neurons by Student's *t* test. *D*, SK2 protein levels in the cerebellum (Cb) and cortex (Cx) are unchanged in $\text{p75}^{-/-}$ mice.

reduced SK tail current could reflect either a compromised SK channel function or an impaired VGCC activity, which would lead to less Ca^{2+} to stimulate SK channels in $\text{p75}^{-/-}$ neurons. To distinguish these possibilities, we measured the current integral of the Ca^{2+} spike complex (induced by the -50 to -30

mV step) but found no significant difference between $\text{p75}^{+/-}$ and $\text{p75}^{-/-}$ neurons (Fig. 3C (b)). We then normalized SK tail currents recorded at -30 mV to the integral of Ca^{2+} spike complex for each neuron individually and found the normalized SK tail currents to be significantly different between

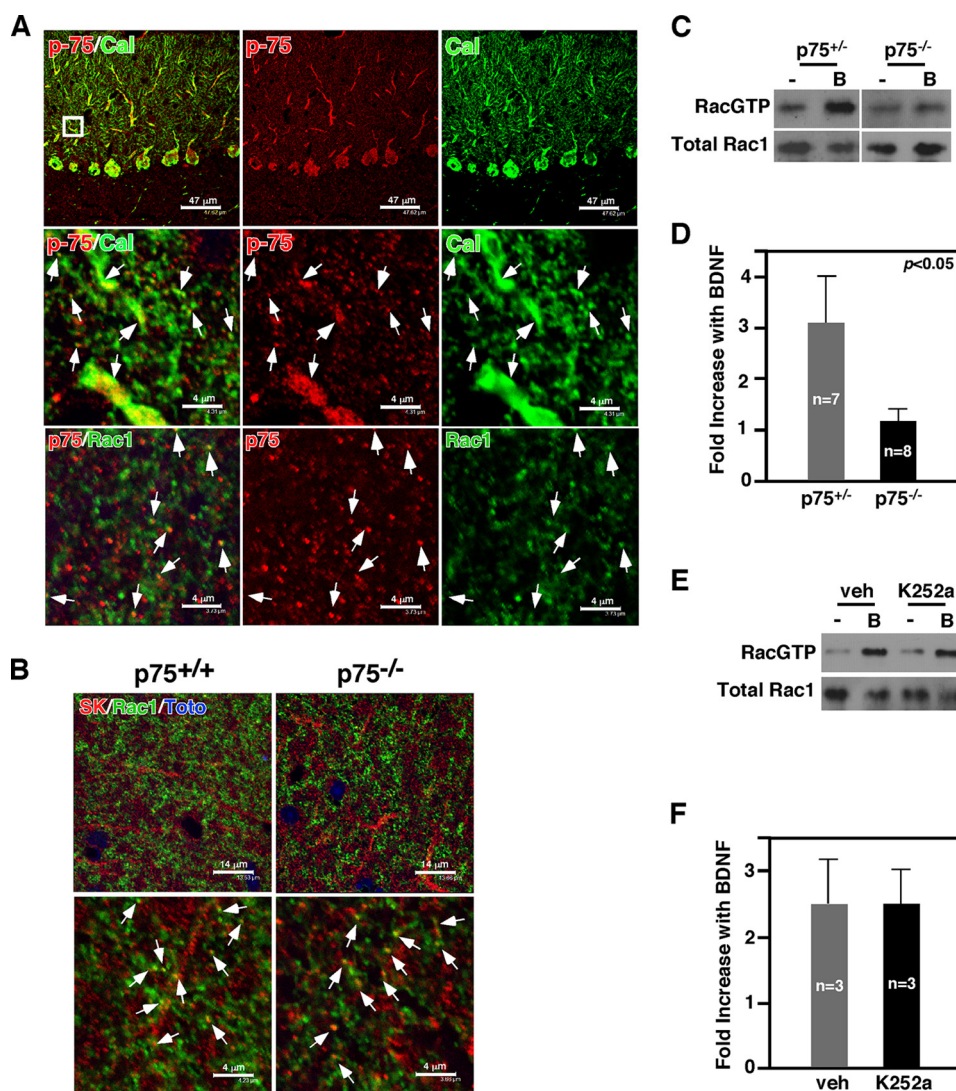


FIGURE 4. p75 is necessary for BDNF-induced Rac1 activation in cerebellar slices. *A*, p75 is expressed in Purkinje cell soma, axons, and dendrites. p75 is expressed in dendritic spines of Purkinje cells. *Arrows* point to colocalization of p75 and calbindin. Also shown is p75 colocalizing with Rac1 in the spines of the cerebellar molecular layer. The *arrows* point to colocalized spines. *B*, SK2 channels are colocalized with Rac1 in the molecular layer of the cerebellum. The *arrows* point to colocalized spines. *C* and *D*, BDNF-induced increase in RacGTP levels in cerebellar slices is attenuated in p75^{-/-} mice compared with heterozygous control littermates. *E* and *F*, inhibition of TrkB did not influence BDNF-induced Rac1 activation in cerebellar slices. In *C* and *E*, *B* indicates BDNF.

p75^{+/-} and p75^{-/-} neurons (Fig. 3C (c)). These results suggest that the reduction in SK tail current in p75^{-/-} neurons most likely reflects a compromised SK channel function rather than a change in VGCC activity. Moreover, because the protein levels of SK2, the major SK isoform in Purkinje neurons (25), were similar between the wild type and p75^{-/-} cerebellum (Figs. 3D and 4B), the observed reduction in SK tail current in p75^{-/-} Purkinje cells is probably due to p75 signaling-mediated modulation of SK channel function in Purkinje cells.

BDNF Activates Rac1 via p75 in Cerebellar Slices—What is the mechanism by which p75 regulates SK channel function in Purkinje cells? Of the signaling pathways that p75 activates, we focused on a small GTPase, Rac1. We have previously reported that p75 activates Rac1 in neural cultures (3, 4). In cultured dorsal root ganglion neurons, Rac1 mediated up-regulation of GIRK channels through increasing phosphatidylinositol 4,5-bisphosphate synthesis, which underlies the neuronal death mechanism activated by p75 cleavage (15). Moreover, Rac1

activity has been shown to play critical roles in regulating dendritic spine morphology in Purkinje cells (36). As Rac1 protein has been detected only among Purkinje cells in the cerebellum (37), we found it to colocalize with p75 and also with SK2 channels in dendritic spines of Purkinje cells in the molecular layer (Fig. 4, A and B). We thus asked whether Rac1 is activated by BDNF, a ligand for p75 that is produced by granule neurons in the cerebellum (38). In acute organotypic cerebellar slices, BDNF increased RacGTP levels within 10 min in the wild type, but failed to do so in p75^{-/-} slices (Fig. 4, C and D). Blocking TrkB activation with 50 nM K252a, a pan-Trk inhibitor, did not attenuate BDNF-mediated Rac1 activation (Fig. 4, E and F), suggesting that p75 is responsible for activating Rac1 in the cerebellum.

Synaptosomes of p75^{-/-} Mice Have Decreased Rac1 Activity—We next asked whether there is any change in steady state RacGTP levels in p75^{-/-} mice compared with wild type *in vivo*. For this, proteins extracted from synaptosome fractions

p75 Regulates SK Channels in Purkinje Cells

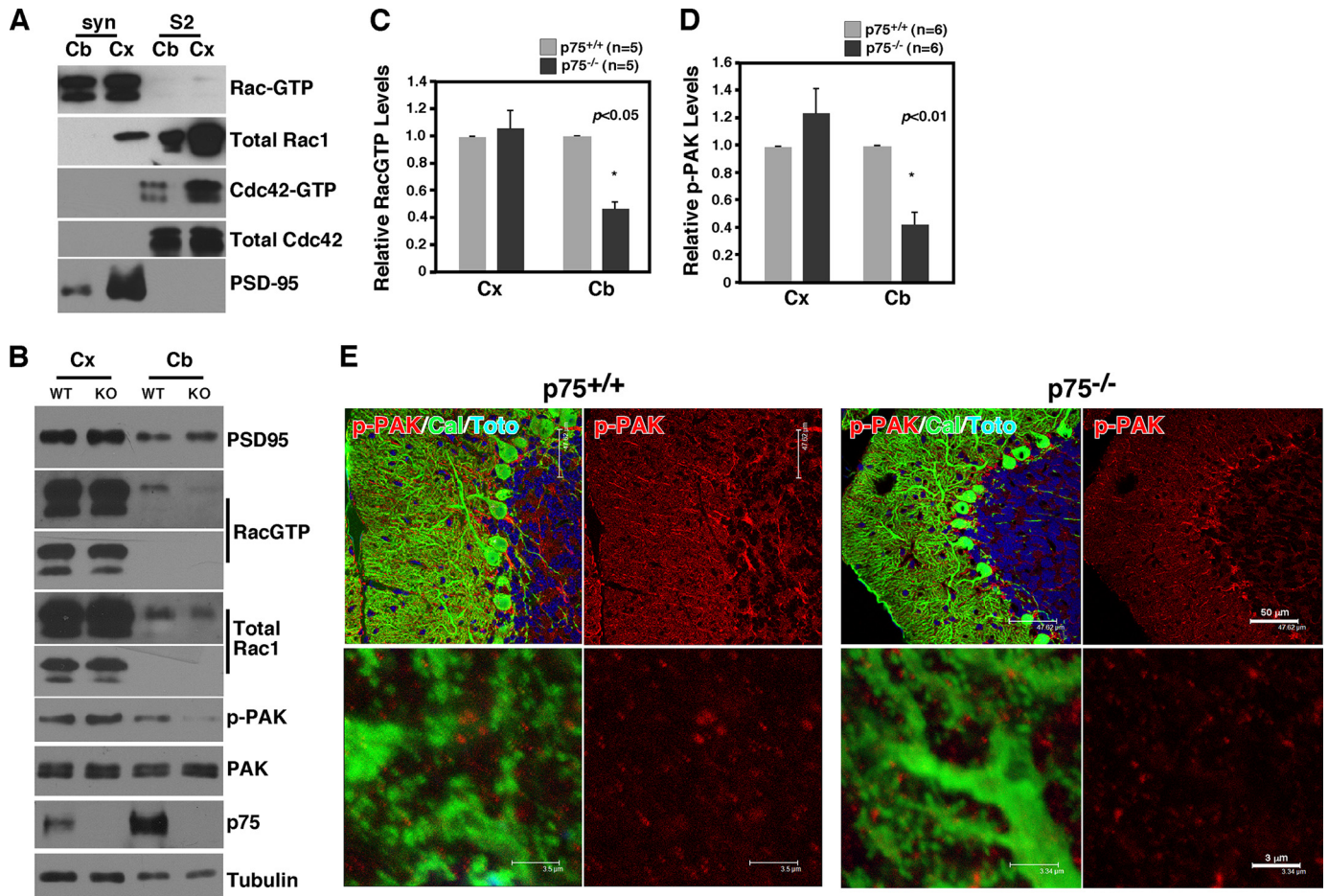


FIGURE 5. Reduction in RacGTP levels in the cerebellum of p75 knock-out mice. A, RacGTP is enriched in the synaptosome fraction. Proteins in synaptosome (Syn) and S2 fractions were subjected to GST-PAK1 pull-down to detect GTP-bound Rac1 prior to Rac1 Western blotting. Note that the majority of Rac1 localized to the synaptosome fraction is GTP-bound. In contrast, Cdc42GTP is predominantly localized to the S2 fraction. PSD95 is a control for the fractionation. Cb, cerebellum; Cx, cortex. B, RacGTP levels and the levels of its downstream effector, p-PAK, are significantly reduced in the cerebellum of p75^{-/-} mice compared with the wild type. Note that the reduction is restricted to the cerebellum and not found in the cortex of the same animal. C, Quantification of RacGTP levels between p75^{+/+} and p75^{-/-} mice. D, Quantification of p-PAK levels between p75^{+/+} and p75^{-/-} mice. E, Images of p-PAK immunohistochemistry in the molecular layer of the cerebellum in p75^{+/+} and p75^{-/-} mice.

from the cerebellum were subjected to RacGTP assays; the remaining cerebral cortices from the same animal were also subjected to the same procedure. It should be noted that in both the cerebral cortex and the cerebellum, active Rac1 was detected almost exclusively in the synaptosome fractions with very little RacGTP detected in the S2 soluble fraction (Fig. 5A). In contrast, active Cdc42 was mostly found in the soluble but not the synaptosome fractions. These results suggest that Rac1 becomes activated preferentially in the synaptic compartments, in agreement with the fact that many guanidine nucleotide exchange factors are also localized to the synaptosomes (39). We found that RacGTP levels were reduced by 60% in the cerebellum from p75^{-/-} mice compared with that in the wild type, whereas there was no difference in the cerebral cortex from the same animals (Fig. 5, B and C). Consistent with the reduction in RacGTP levels, p-PAK levels were also reduced only in the cerebellum (Fig. 5, B and D). Although PAK undergoes autophosphorylation when bound to both Rac1GTP and Cdc42GTP (40), p-PAK levels in the synaptosome represent mostly Rac1 activation, because Cdc42GTP is detected mainly in soluble fractions (Fig. 5A). Because p75 is colocalized with Rac1 in dendritic spines in the molecular layer (Fig. 4A) and in syn-

aptosome fractions of the cerebellum (Fig. 5B), these results suggest that Rac1 activation and its downstream signaling are compromised in synaptic compartments of the p75^{-/-} cerebellum.

Immunohistochemical analysis also revealed the presence of p-PAK in dendritic spines in the molecular layer and a reduction of its levels in p75^{-/-} mice (Fig. 5E). p-PAK immunoreactivity was also detected in Bergmann glia, based on their longitudinal morphology, in agreement with a report that Rac1 activation within Bergmann glia regulated ensheathment of Purkinje cell spines (41). p75 is, however, not expressed in Bergmann glia (Fig. 4A). Along with the Western blotting data, these results together suggest that p75 regulates Rac1 activity in synaptic compartments of Purkinje cells.

Rac1 Inhibition Attenuates SK-mediated Tail Current in Purkinje Cells—Because SK channel and Rac1 activity are colocalized in dendritic spines in the molecular layer of the cerebellum (Fig. 4), we next asked whether Rac1 modulates SK channel function in Purkinje cells. For this, SK channel-mediated tail currents were recorded as in Fig. 3 but in the presence of 100 μ M NSC23766, a Rac1 inhibitor. Bath perfusion of NSC23766 markedly changed the waveform of the SK channel-mediated

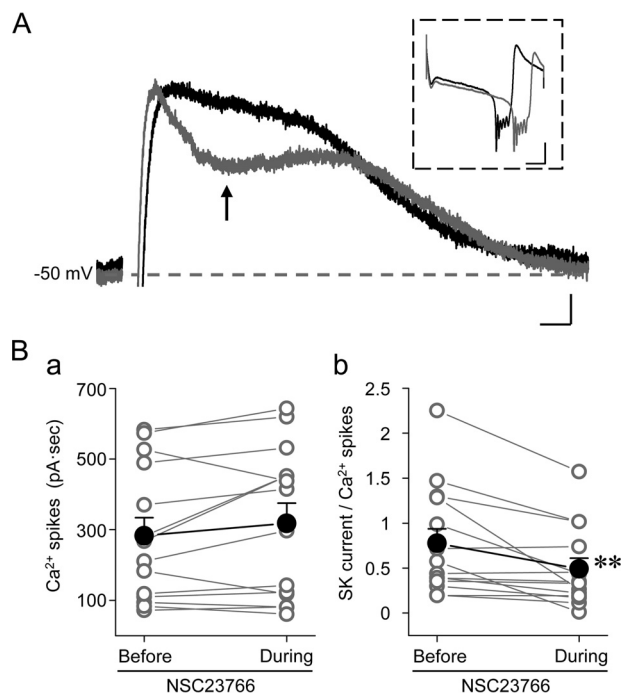


FIGURE 6. SK channel activity is regulated by Rac1 in Purkinje cells. *A*, representative traces of SK-mediated tail currents in a WT Purkinje cell before (*black*) and during (*gray*) bath application of 100 μM NSC23766. The same protocol was used as in Fig. 3A (*a*). The *arrow* indicates the point of maximal inhibition, from where the inhibitory effect of NSC23766 was measured for data analysis. The *inset* shows Ca^{2+} spike complexes from the same records. Scale bars, 30 ms, 20 pA; 50 ms, 300 pA for *inset*. *B*, individual (*open circles*) and summary data (*filled circles*) for integral currents of Ca^{2+} spike complexes (*B (a)*) and amplitudes of SK-mediated tail currents at the point indicated in *A* normalized to the integral currents of Ca^{2+} spike complexes (*B (b)*) before and during the treatment with NSC23766. **, $p < 0.01$, paired *t* test ($n = 14$).

tail currents, leading to a fast, but partial, decrease right after the tail current had reached its peak (Fig. 6A). NSC23766 application also appeared to have a moderate effect on the Ca^{2+} spike complex evoked by the preceding voltage step (Fig. 6A, *inset*), showing an average increase of 11% based on the current integral of the Ca^{2+} spike complex (Fig. 6B (*a*)). This increase, however, was not statistically significant. On the other hand, NSC23766 caused a significant reduction in SK-mediated tail current by $\sim 28\%$ ($p < 0.01$) after normalization to the integral of Ca^{2+} spike complex for the same cells (Fig. 6B (*b*)). It should be noted that because the data were normalized against the current integral of the Ca^{2+} spike complex from the same trace, this assessment largely excludes the possibility that altered SK currents were due to NSC23766-induced changes in VGCC activities in Purkinje cells. The above data thus suggest that Rac1 activity contributes positively to normal SK channel activities in Purkinje cells. Taken together with the findings that both RacGTP levels and the SK channel-mediated tail currents are reduced in $p75^{-/-}$ mice, it is highly likely that p75-dependent Rac1 activity provides the functional link between p75 and SK channels in Purkinje cells.

Acute Rac1 Inhibition Disrupts Firing Regularity and Enhances Purkinje Cell Firing Rate—If Rac1 indeed mediates the effect of p75 modulation of SK channels in Purkinje cells, then blocking Rac1 should also alter Purkinje cell firing in a similar fashion as inhibiting SK channels. It has been reported that SK channels play an important role in limiting the maximum firing rate of

Purkinje cells. Blocking SK channels in the cerebellum has been shown to increase the Purkinje cell firing rate to up to 500 Hz and to cause them to fire irregularly (29). SK channels also play a part in the AHP following action potential bursts and reduce excitatory postsynaptic potential in Purkinje cell dendrites (42). To test whether acute blockade of Rac1 also alters Purkinje cell firing, we used both extracellular and whole-cell current clamp recordings to monitor firing pattern changes in response to Rac1 blockade by NSC23766. Bath perfusion of NSC23766 in extracellular recordings to tonically firing Purkinje cells dramatically increased the firing frequency and caused them to fire either irregularly (10 of 15 cells tested; see Fig. 7A (*b*) for an example) or phasically (5 of 15 cells; data not shown, but in a similar pattern as Fig. 1D). Next, we applied NSC23766 intracellularly through the patch pipette with the whole-cell current clamp recording. This resulted in dramatic changes in the firing pattern 60 s after the establishment of the whole-cell configuration (Fig. 7B). Presumably, it took about 60 s for NSC23766 to diffuse to the dendritic trees of the patched cells. Thus, the firing pattern changes appeared to be more robust in whole-cell than in extracellular recordings, probably because of the enhanced intracellular access of NSC23766 in the formal configuration. Importantly, burst firing with super fast instantaneous firing frequencies (400–1000 Hz) was obtained in $\sim 50\%$ of Purkinje cells (3 of 6 cells tested; the remaining 3 cells exhibited enhanced firing rates without obvious burst) with the block of Rac1 by intracellular dialysis of NSC23766 in the current clamp mode (Fig. 7B (*d*)). Moreover, the dialysis of NSC23766 reduced the AHP amplitude of Purkinje cells by $\sim 20.9\%$ (Fig. 7B (*e* and *f*); from 14.8 ± 1.3 to 11.7 ± 1.4 mV), which could account for the increased firing rate and the conversion to burst firing. This modulation of AHP by NSC23766 also resembles that by apamin in tonic firing cerebellar Purkinje cells. Together, these results demonstrate that blocking Rac1 elicits changes in Purkinje cell firing patterns that are comparable to those elicited by inhibition of SK channels, further supporting the role of Rac1 in modulating SK channel activity in Purkinje cells and its involvement in p75 modulation of Purkinje cell firing.

Purkinje Cells from $p75^{-/-}$ Mice Exhibit Decreased Spine Density and Altered Spine Morphology—It should be noted that acute inhibition of Rac1 did not evoke exactly the same change in Purkinje cell firing as the global knock-out of p75 expression, despite the demonstrated involvement of SK channels in both situations. Most likely, the structural and long term effects of the p75-Rac1 pathway on spine development and morphology could account for the difference. It is well known that BDNF signaling has a profound effect on Purkinje cell morphology. In $\text{BDNF}^{-/-}$ mice, Purkinje cells fail to develop normal dendritic trees and exhibit a foliation defect specifically in lobules VI and VII (43). Deleting p75 from $\text{BDNF}^{+/+}$ mice worsened the foliation defect (2). However, to what extent p75 knockout alone affects Purkinje cell morphology was not known. Therefore, we performed morphological analysis for $p75^{+/+}$ and $p75^{-/-}$ Purkinje neurons using Golgi staining. As shown in representative images in Fig. 8A, there was no obvious defect in the overall dendritic arborization in the absence of p75; Purkinje cells in $p75^{-/-}$ mice were planar in organization, reaching the pial surface to a similar extent as in the wild type. The spine density in

p75 Regulates SK Channels in Purkinje Cells

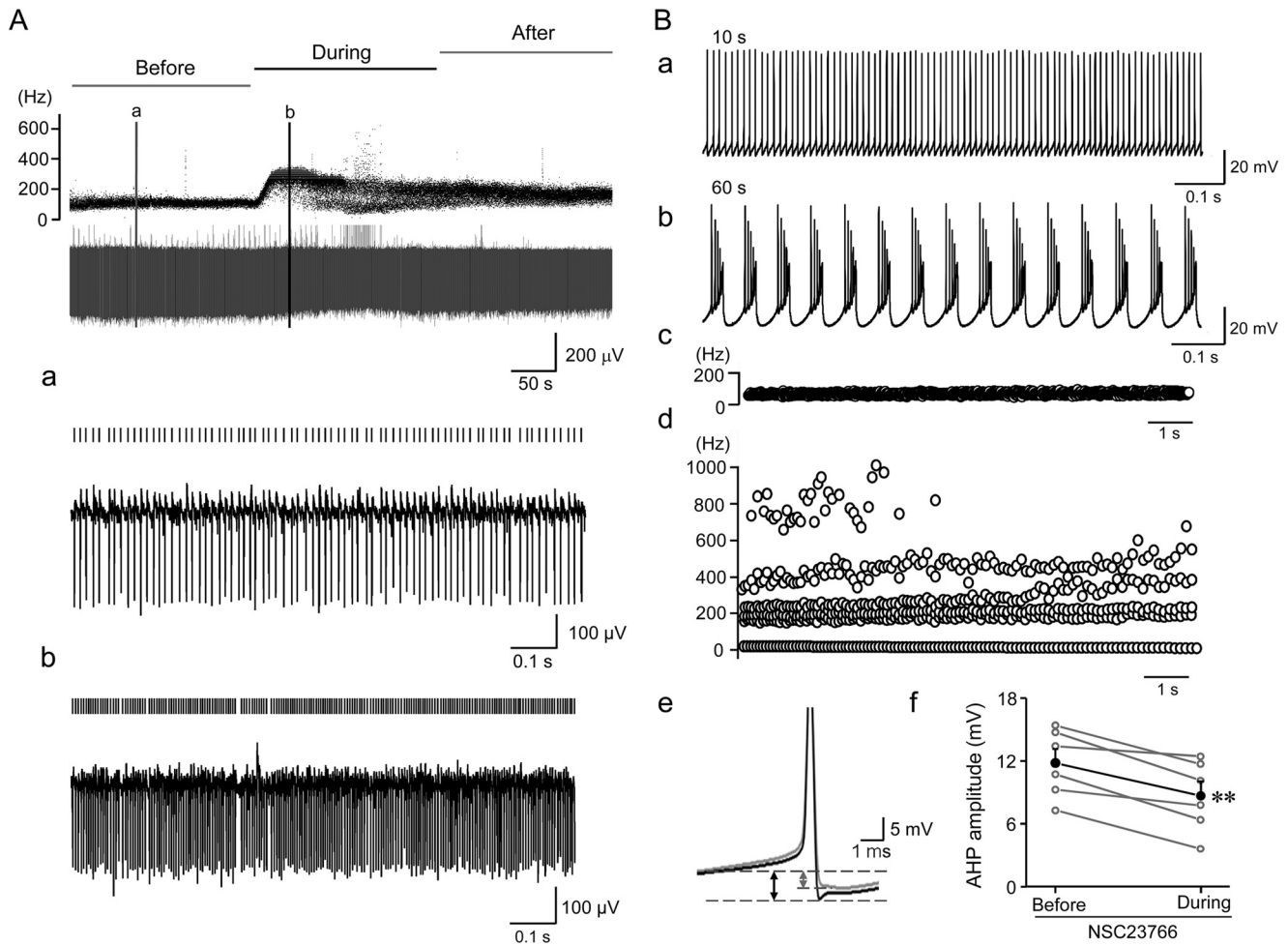


FIGURE 7. Rac1 inhibition alters Purkinje cell firing. *A*, extracellular recording of Purkinje cell firing before, during, and after application of Rac1 inhibitor ($100 \mu\text{M}$ NSC23766). *Top traces*, instantaneous firing frequency (Hz); *bottom traces*, field potential (μV) changes. Activities before and during bath perfusion of $100 \mu\text{M}$ NSC23766 at the time points indicated by the two vertical lines in the top panel are expanded in *a* and *b*. Each firing spike is indicated by a short vertical line above the potential trace. Note the accelerated firing rate and irregularity during NSC23766 application. *B*, effect of intracellular dialysis of NSC23766 ($100 \mu\text{M}$) on Purkinje cell firing and AHP amplitude in whole-cell current clamp recordings. NSC23766 was delivered through the recording pipette to the cytoplasm of the Purkinje cell in the cerebellar slice. No holding current was applied. Membrane potential changes at 10 s (*a*) and 60 s (*b*) after establishment of the whole-cell configuration are shown to demonstrate different firing patterns before and after Rac1 inhibition. Note the transition from tonic firing (*a*) to burst firing (*b*). Instantaneous firing frequencies during 10–20 s (*c*) were low and regular but became highly variable during 60–70 s (*d*). Note that the instantaneous firing frequency reached 800 Hz during Rac1 inhibitor treatment. *B* (*e*), peak truncated action potentials highlighting AHP (indicated by the dashed lines and arrows) at ~ 10 s (*black*) and ~ 60 s (*gray*) during pipette dialysis of NSC23766. Each trace represents the average of 200 action potentials. *B* (*f*), mean AHP amplitudes at 10 and 60 s after establishment of whole-cell configuration with the pipettes containing NSC23766. The average reduction (filled circles and black line) was 3.1 mV. **, $p < 0.01$, paired *t* test.

the secondary and tertiary dendritic branches, however, was decreased by 25% in $p75^{-/-}$ mice compared with the wild type littermates (Fig. 8, *B* and *C*). Using electron microscopy, with representative images shown in Fig. 8*D*, morphological changes were also observed in the spine head area, which were increased by 21% (Fig. 8*E*). The change in spine length was not statistically significant. These results agree with the reports that the loss of p75 or blocking its signaling resulted in changes in spine density in hippocampal neurons both *in vivo* (44) and *in vitro* in response to BDNF (45). On the other hand, these results are opposite to the phenotypes obtained when a constitutively active Rac1 was genetically introduced to Purkinje cells, wherein the number of dendritic spines was increased and spines became smaller compared with those in the wild type (36). We interpret these results as an additional support for our data that Rac1 activity is attenuated in $p75^{-/-}$ mice and conclude that in addition to modulating SK channel function, p75

signaling also contributes to structural changes in Purkinje cell dendritic spines during development and plasticity, which may explain the difference in acute Rac1 inhibition and global p75 depletion upon Purkinje cell firing.

DISCUSSION

The current study demonstrates that cerebellar Purkinje cells of $p75^{-/-}$ mice exhibit defects in firing properties, due to diminished SK channel function. We attribute this to the ability of p75 to activate Rac1, because RacGTP levels are reduced in the $p75^{-/-}$ cerebellum, and inhibiting Rac1 attenuated SK-mediated tail currents to a similar extent as in $p75^{-/-}$ Purkinje cells in cerebellar slices (28% by NSC23766 and 21% in $p75^{-/-}$ mice). Because SK channel activity is critically involved in maintaining firing regularity in Purkinje cells (29), our results suggest that p75 is involved in maintaining normal spontaneous

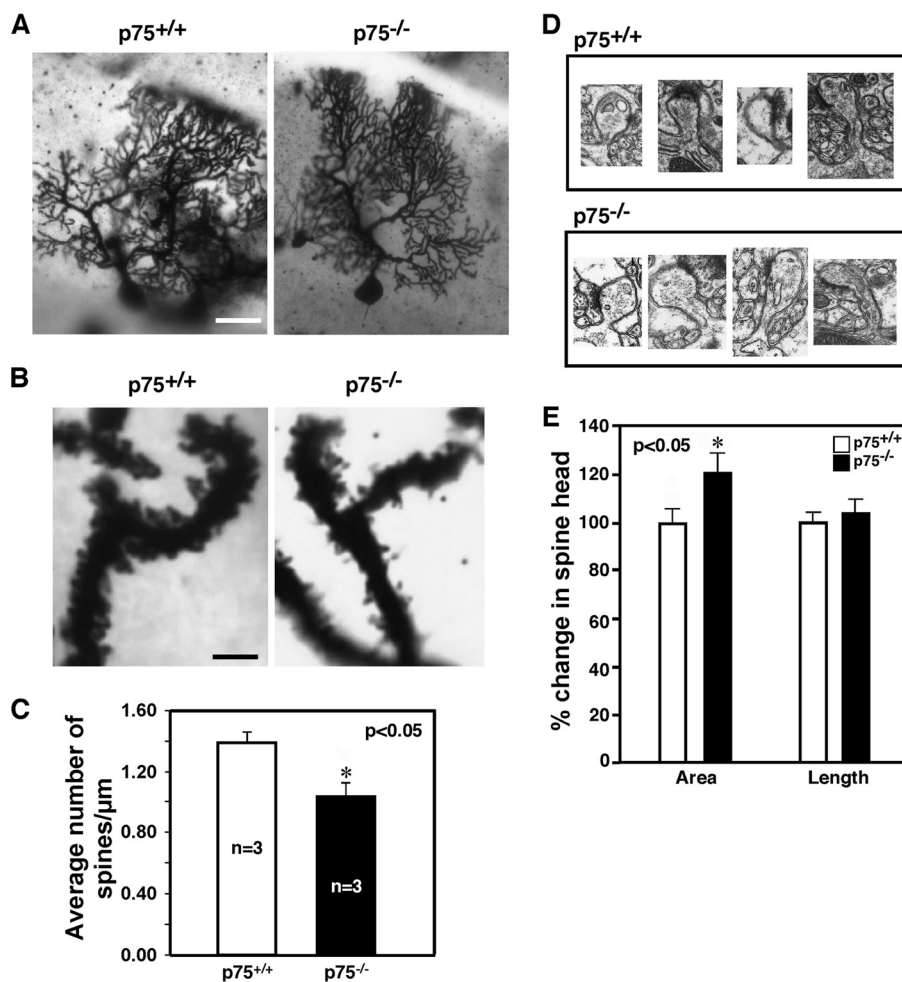


FIGURE 8. Reduction in the number of spines in Purkinje cells in the absence of p75. *A*, representative images of Purkinje cells stained with Golgi from adult p75^{+/+} and p75^{-/-} mice. Scale bar, 25 μm . *B*, representative images of Purkinje cell dendrites that were used for quantification of spines. Scale bar, 6 μm . *C*, quantification of the number of spines. Five Purkinje neurons in lobules 4, 5, 6, and 7 per mouse were analyzed using the NeuroLucida[®] version 7 image analysis system (MBF Biosciences), and the spine density was estimated ($n = 3$ mice). For each Purkinje neuron, at least five different secondary and tertiary dendritic branches were randomly selected for spine analysis at $\times 100$ magnification to obtain the estimated values for the number of spines in a given length. *D*, representative EM images of Purkinje cell spines from adult p75^{+/+} and p75^{-/-} mice. *E*, quantification of spine area and spine length based on EM images collected from three different sets of mice and a total of 29 spines with features of post-synaptic density (PSD) using ImageJ.

firing of cerebellar Purkinje cells, in part by activating Rac1, which in turn regulates SK channels.

We demonstrated that BDNF activated Rac1 primarily through p75 in organotypic cerebellar slices; BDNF did not increase RacGTP levels in p75^{-/-} mice, and inhibiting TrkB with K252a had no effect on Rac1 activation by BDNF. Is BDNF then the neurotrophin that activates Rac1 signaling via p75, thereby regulating Purkinje cell firing frequency? Our attempt to measure BDNF-induced changes in Purkinje cell firing frequency did not give consistent results that were interpretable (data not shown). This could be due to a simultaneous activation of resident TrkB, which could also elicit diverse signaling events that could counteract the effect of p75 on spontaneous firing, such as activating the phospholipase C γ pathway (46, 47) or different ion channels (48, 49). It is also possible that bath application of BDNF might have failed to replicate the *in vivo* time course of its action, which can be very fast like that of neurotransmitters (49, 50). Alternatively, it could also result from differential effects of BDNF as a paracrine or autocrine factor onto Purkinje cells. BDNF is produced in the cerebellum

by both granule neurons and Purkinje cells (43). As a paracrine factor released from granule neurons, BDNF plays a role in paired pulse facilitation in response to parallel fiber stimulation, which is impaired in Purkinje cells of BDNF^{-/-} mice (51). However, because the changes in spontaneous firing frequency in p75^{-/-} Purkinje cells were observed in the presence of both AMPA and GABA_A receptor blockers, it is more likely that the altered function is a response to the autocrine action of BDNF.

p75 can elicit multiple signaling pathways besides Rac1, such as JNK, RhoA, and NF- κ B (1). It is thus possible that a signaling pathway(s) other than Rac1 was evoked to regulate SK channel activity. However, we argue that p75-mediated Rac1 activation is most likely responsible for the observed changes in SK channel function and regularity of spontaneous firing in Purkinje cells for the following reasons. 1) RacGTP levels are significantly reduced in p75 null mice in the cerebellar synaptosomes, where p75 is also located. In the cortex, where p75 is detected at a much lower level in the synaptic compartments, RacGTP levels were the same between the wild type and p75^{-/-} mice. 2) Unlike Cdc42 and RhoA, RacGTP is detected almost exclu-

p75 Regulates SK Channels in Purkinje Cells

sively in synaptosomes in the brain. 3) BDNF increased RacGTP levels in organotypic cerebellar slices by activating p75 but not TrkB. 4) Inhibiting Rac1 activation with NSC23766 reduced the SK channel-mediated tail current to a similar extent as that found in p75^{-/-} mice, and it altered Purkinje cell firing and reduced AHP amplitude similarly as pharmacological blockade of SK channels *in vitro* (29, 42). Additionally, we did not detect any change in any other signaling pathway that p75 is known to activate, such as JNK activity, RhoAGTP, and Cdc42GTP levels in the cerebellum (data not shown). We also postulate that the observed reduction in spine density in p75^{-/-} Purkinje cells is probably due to the reduction in RacGTP levels, because constitutive activation of Rac1 in Purkinje cells led to an increase in spine density (36).

It should be noted that although NSC23766 reduced AHP amplitude, we did not observe a significant change of AHP in p75^{-/-} Purkinje neurons. This could be due to the fact that SK channels have opposite effects on AHP, depending on whether Purkinje cells fire bursts or tonically; apamin reduced AHP amplitude during tonic firing but enhanced it during burst firing, albeit with an accelerated decay (29). In particular, when SK channel activity is inhibited by ~23%, as in the case of p75^{-/-} neurons, it becomes more difficult to detect changes in AHP. It is also possible that other channels compensated for the reduced SK channel function in p75^{-/-} Purkinje cells during development, negating the effect on AHP.

Cerebellar granule neurons express high levels of p75 until they migrate inward and form the internal granular cell layer. We thus cannot rule out the possibility that the loss of p75 in granule neurons during development has influenced them in a way that affected the formation of functional synapses and thereby proper spine formation in Purkinje cells. For instance, it was shown recently that pro-BDNF activates p75, thereby inhibiting granule cell migration (52). Although it remains to be determined whether pro-BDNF is indeed released as a p75 ligand in the cerebellum (53, 54), BDNF was shown to modulate migration of granule neurons because their migration was delayed in BDNF^{-/-} mice (55). This effect was, however, dependent on TrkB rather than p75 (56). Because the internal granular cell layer is formed normally in p75^{-/-} mice, and there is no obvious defect in the external granular cell layer or internal granular cell layer (2), it is unlikely that p75 plays a major role in granule neuron migration during development. We should also point out that we used the wild type and p75 null littermates after granule cell migration is complete, P15–P25, and we did not observe any age-dependent changes in the firing frequency or RacGTP levels (data not shown). Obviously, analysis of mice wherein p75 was conditionally deleted in granule neurons or Purkinje cells will be necessary to address the question fully.

How does Rac1 activity impinge on SK channels? Rac1 has been shown to regulate K⁺ channel activities, such as the ether-a-go-go-related potassium channel in a rat pituitary cell line (57), the inwardly rectifying K⁺ channel, Kir2.1 (12), and the ATP-sensitive K⁺ channels (58), but the underlying mechanisms can be quite different. Current literature suggests that Rac1 affects K⁺ channel function indirectly by regulating either channel trafficking to the plasma membrane through associa-

tion with the actin cytoskeleton (59–62) or channel internalization (12). Also, the p75-evoked activation of Rac1 could promote phosphatidylinositol 5-kinase activity for enhanced phosphatidylinositol 4,5-bisphosphate synthesis and, in turn, activation of GIRK channels (63). Similar mechanisms could be at play for SK channels in Purkinje cells. Alternatively, it has been shown that the SK3 channel interacts with N-WASP protein in neural stem cells (63). WASP (Wiskott-Aldrich syndrome protein) provides scaffolds that activate the Arp2/3 complex in response to RhoGTPases and other upstream signals (64, 65). WAVE1/2 have been implicated in the stimulatory effect of Rac1 on epithelial Na⁺ channels in principal cells of the kidney cortical collecting duct (66), whereas inhibition of WAVE1 via phosphorylation by cyclin-dependent kinase 5 was shown to reduce dendritic spine density in mouse neurons (67). Given that Rac1 activity was largely impaired due to the loss of p75, the decreased spine density found in p75^{-/-} Purkinje neurons could suggest a reduction in Rac1-dependent WAVE activity. This activity may also be important for maintaining SK channel function in Purkinje cells if the SK3-nWASP interaction can be extrapolated to related WAVE proteins and SK2, the principal SK isoform in Purkinje cells (25).

Spontaneous firing in Purkinje cells is believed to play a role in pacemaking, relaying time-dependent motor information rapidly and with high precision (35, 68). In ataxic *ducky* and *tottering* mice that harbor mutations in P/Q-type VGCCs, SK channel activity in Purkinje cell dendrites was reduced, resulting in decreased AHP amplitude and irregular firing (70). The finding that SK channel activator, 1-ethyl-2-benzimidazolinone, not only restored Purkinje cell firing regularity but also improved the ataxic phenotype of the mutant mice highlights the contribution of SK channels in maintenance of Purkinje cell pacemaking and normal motor coordination. Little or no information is available, however, on whether and how SK channels are regulated by signal transduction pathways that are known to modulate Purkinje cell development and function. Our study reveals that in addition to responding to Ca²⁺ signal coming from VGCCs, the SK channel activity is further modulated by neurotrophins utilizing the p75-Rac1 signaling cascade. It also suggests a mechanism by which neurotrophins exert their action on Purkinje cell firing, thereby fine-tuning motor control and cognitive processing. One might then expect an ataxic phenotype in p75^{-/-} mice. Indeed, disrupting the p75 gene via targeting its fourth exon resulted in mild ataxia (23). The p75^{-/-} mice that were targeted via its third exon, which we have used for this study, also exhibited motor defect in the rotarod assays (data not shown). However, because these mice develop sores in their feet, it is difficult to ascertain whether the attenuated response in rotarod tests is solely due to p75 function in the cerebellum. Conditional deletion of p75 in Purkinje cells will help to address the question.

REFERENCES

1. Chao, M. V. (2003) Neurotrophins and their receptors: a convergence point for many signalling pathways. *Nat. Rev. Neurosci.* **4**, 299–309
2. Carter, A. R., Berry, E. M., and Segal, R. A. (2003) Regional expression of p75NTR contributes to neurotrophin regulation of cerebellar patterning. *Mol. Cell Neurosci.* **22**, 1–13
3. Harrington, A. W., Kim, J. Y., and Yoon, S. O. (2002) Activation of Rac

- GTPase by p75 is Necessary for c-Jun N-terminal kinase-mediated apoptosis. *J. Neurosci.* **22**, 156–166
4. Tep, C., Kim, M. L., Opincariu, L. I., Limpert, A. S., Chan, J. R., Appel, B., Carter, B. D., and Yoon, S. O. (2012) BDNF induces polarized signaling of small GTPase (Rac1) at the onset of Schwann cell myelination through partitioning-defective 3 (Par3). *J. Biol. Chem.* **287**, 1600–1608
 5. de Curtis, I. (2008) Functions of Rac GTPases during neuronal development. *Dev. Neurosci.* **30**, 47–58
 6. Xie, Z., Photowala, H., Cahill, M. E., Srivastava, D. P., Woolfrey, K. M., Shum, C. Y., Haganir, R. L., and Penzes, P. (2008) Coordination of synaptic adhesion with dendritic spine remodeling by AF-6 and kalirin-7. *J. Neurosci.* **28**, 6079–6091
 7. Toliás, K. F., Bikoff, J. B., Burette, A., Paradis, S., Harrar, D., Tavazoie, S., Weinberg, R. J., and Greenberg, M. E. (2005) The Rac1-GEF Tiam1 couples the NMDA receptor to the activity-dependent development of dendritic arbors and spines. *Neuron* **45**, 525–538
 8. Toliás, K. F., Bikoff, J. B., Kane, C. G., Toliás, C. S., Hu, L., and Greenberg, M. E. (2007) The Rac1 guanine nucleotide exchange factor Tiam1 mediates EphB receptor-dependent dendritic spine development. *Proc. Natl. Acad. Sci. U.S.A.* **104**, 7265–7270
 9. Buttery, P., Beg, A. A., Chih, B., Broder, A., Mason, C. A., and Scheiffele, P. (2006) The diacylglycerol-binding protein α 1-chimaerin regulates dendritic morphology. *Proc. Natl. Acad. Sci. U.S.A.* **103**, 1924–1929
 10. Van de Ven, T. J., VanDongen, H. M., and VanDongen, A. M. (2005) The nonkinase phorbol ester receptor α 1-chimerin binds the NMDA receptor NR2A subunit and regulates dendritic spine density. *J. Neurosci.* **25**, 9488–9496
 11. Oh, D., Han, S., Seo, J., Lee, J. R., Choi, J., Groffen, J., Kim, K., Cho, Y. S., Choi, H. S., Shin, H., Woo, J., Won, H., Park, S. K., Kim, S. Y., Jo, J., Whitcomb, D. J., Cho, K., Kim, H., Bae, Y. C., Heisterkamp, N., Choi, S. Y., and Kim, E. (2010) Regulation of synaptic Rac1 activity, long-term potentiation maintenance, and learning and memory by BCR and ABR Rac GTPase-activating proteins. *J. Neurosci.* **30**, 14134–14144
 12. Boyer, S. B., Slesinger, P. A., and Jones, S. V. (2009) Regulation of Kir2.1 channels by the Rho-GTPase, Rac1. *J. Cell Physiol.* **218**, 385–393
 13. Meyer, D. K., Olenik, C., Hofmann, F., Barth, H., Leemhuis, J., Brünig, I., Aktories, K., and Nörenberg, W. (2000) Regulation of somatodendritic GABA_A receptor channels in rat hippocampal neurons: evidence for a role of the small GTPase Rac1. *J. Neurosci.* **20**, 6743–6751
 14. Wilk-Blaszczak, M. A., Singer, W. D., Quill, T., Miller, B., Frost, J. A., Sternweis, P. C., and Belardetti, F. (1997) The monomeric G-proteins Rac1 and/or Cdc42 are required for the inhibition of voltage-dependent calcium current by bradykinin. *J. Neurosci.* **17**, 4094–4100
 15. Coulson, E. J., May, L. M., Osborne, S. L., Reid, K., Underwood, C. K., Meunier, F. A., Bartlett, P. F., and Sah, P. (2008) p75 neurotrophin receptor mediates neuronal cell death by activating GIRK channels through phosphatidylinositol 4,5-bisphosphate. *J. Neurosci.* **28**, 315–324
 16. Li, Z., Aizenman, C. D., and Cline, H. T. (2002) Regulation of rho GTPases by crossstalk and neuronal activity *in vivo*. *Neuron* **33**, 741–750
 17. Sin, W. C., Haas, K., Ruthazer, E. S., and Cline, H. T. (2002) Dendrite growth increased by visual activity requires NMDA receptor and Rho GTPases. *Nature* **419**, 475–480
 18. Penzes, P., Beeser, A., Chernoff, J., Schiller, M. R., Eipper, B. A., Mains, R. E., and Haganir, R. L. (2003) Rapid induction of dendritic spine morphogenesis by trans-synaptic ephrinB-EphB receptor activation of the Rho-GEF kalirin. *Neuron* **37**, 263–274
 19. Hayashi-Takagi, A., Takaki, M., Graziane, N., Seshadri, S., Murdoch, H., Dunlop, A. J., Makino, Y., Seshadri, A. J., Ishizuka, K., Srivastava, D. P., Xie, Z., Baraban, J. M., Houslay, M. D., Tomoda, T., Brandon, N. J., Kamiya, A., Yan, Z., Penzes, P., and Sawa, A. (2010) Disrupted-in-Schizophrenia 1 (DISC1) regulates spines of the glutamate synapse via Rac1. *Nat. Neurosci.* **13**, 327–332
 20. Chen, L. Y., Rex, C. S., Babayan, A. H., Kramár, E. A., Lynch, G., Gall, C. M., and Lauterborn, J. C. (2010) Physiological activation of synaptic Rac>PAK (p-21 activated kinase) signaling is defective in a mouse model of fragile X syndrome. *J. Neurosci.* **30**, 10977–10984
 21. Lee, K. F., Li, E., Huber, L. J., Landis, S. C., Sharpe, A. H., Chao, M. V., and Jaenisch, R. (1992) Targeted mutation of the gene encoding the low affinity NGF receptor p75 leads to deficits in the peripheral sensory nervous system. *Cell* **69**, 737–749
 22. Bentley, C. A., and Lee, K. F. (2000) p75 is important for axon growth and schwann cell migration during development. *J. Neurosci.* **20**, 7706–7715
 23. von Schack, D., Casademunt, E., Schweigreiter, R., Meyer, M., Bibel, M., and Dechant, G. (2001) Complete ablation of the neurotrophin receptor p75NTR causes defects both in the nervous and the vascular system. *Nat. Neurosci.* **4**, 977–978
 24. del Río, J. A., and Soriano, E. (2010) Regenerating cortical connections in a dish: the entorhino-hippocampal organotypic slice co-culture as tool for pharmacological screening of molecules promoting axon regeneration. *Nat. Protoc.* **5**, 217–226
 25. Cingolani, L. A., Gymnopoulos, M., Boccaccio, A., Stocker, M., and Pedarzani, P. (2002) Developmental regulation of small-conductance Ca²⁺-activated K⁺ channel expression and function in rat Purkinje neurons. *J. Neurosci.* **22**, 4456–4467
 26. Sah, P. (1992) Role of calcium influx and buffering in the kinetics of Ca²⁺-activated K⁺ current in rat vagal motoneurons. *J. Neurophysiol.* **68**, 2237–2247
 27. Constanti, A., and Sim, J. A. (1987) Calcium-dependent potassium conductance in guinea-pig olfactory cortex neurones *in vitro*. *J. Physiol.* **387**, 173–194
 28. Womack, M., and Khodakhah, K. (2002) Active contribution of dendrites to the tonic and trimodal patterns of activity in cerebellar Purkinje neurons. *J. Neurosci.* **22**, 10603–10612
 29. Womack, M. D., and Khodakhah, K. (2003) Somatic and dendritic small-conductance calcium-activated potassium channels regulate the output of cerebellar Purkinje neurons. *J. Neurosci.* **23**, 2600–2607
 30. Swensen, A. M., and Bean, B. P. (2003) Ionic mechanisms of burst firing in dissociated Purkinje neurons. *J. Neurosci.* **23**, 9650–9663
 31. Womack, M. D., Hoang, C., and Khodakhah, K. (2009) Large conductance calcium-activated potassium channels affect both spontaneous firing and intracellular calcium concentration in cerebellar Purkinje neurons. *Neuroscience* **162**, 989–1000
 32. Castle, N. A., Haylett, D. G., and Jenkinson, D. H. (1989) Toxins in the characterization of potassium channels. *Trends Neurosci.* **12**, 59–65
 33. Faber, E. S., and Sah, P. (2002) Physiological role of calcium-activated potassium currents in the rat lateral amygdala. *J. Neurosci.* **22**, 1618–1628
 34. Womack, M. D., and Khodakhah, K. (2004) Dendritic control of spontaneous bursting in cerebellar Purkinje cells. *J. Neurosci.* **24**, 3511–3521
 35. De Zeeuw, C. I., Hoebeek, F. E., Bosman, L. W. J., Schonewille, M., Witter, L., and Koekoek, S. K. (2011) Spatiotemporal firing patterns in the cerebellum. *Nat. Rev. Neurosci.* **12**, 327–344
 36. Luo, L., Hensch, T. K., Ackerman, L., Barbel, S., Jan, L. Y., and Jan, Y. N. (1996) Differential effects of the Rac GTPase on Purkinje cell axons and dendritic trunks and spines. *Nature* **379**, 837–840
 37. Richard, V., Dulon, D., and Hafidi, A. (2008) Expression of Rho GTPases Rho-A and Rac1 in the adult and developing gerbil cerebellum. *Int. J. Dev. Neurosci.* **26**, 723–732
 38. Rocamora, N., García-Ladona, F. J., Palacios, J. M., and Mengod, G. (1993) Differential expression of brain-derived neurotrophic factor, neurotrophin-3, and low-affinity nerve growth factor receptor during the postnatal development of the rat cerebellar system. *Brain Res. Mol. Brain Res.* **17**, 1–8
 39. Penzes, P., Johnson, R. C., Sattler, R., Zhang, X., Haganir, R. L., Kambampati, V., Mains, R. E., and Eipper, B. A. (2001) The neuronal Rho-GEF Kalirin-7 interacts with PDZ domain-containing proteins and regulates dendritic morphogenesis. *Neuron* **29**, 229–242
 40. Manser, E., Huang, H. Y., Loo, T. H., Chen, X. Q., Dong, J. M., Leung, T., and Lim, L. (1997) Expression of constitutively active α -PAK reveals effects of the kinase on actin and focal complexes. *Mol. Cell Biol.* **17**, 1129–1143
 41. Lippman, J. J., Lordkipanidze, T., Buell, M. E., Yoon, S. O., and Dunaevsky, A. (2008) Morphogenesis and regulation of Bergmann glial processes during Purkinje cell dendritic spine ensheathment and synaptogenesis. *Glia* **56**, 1463–1477
 42. Hossy, E., Piochon, C., Teuling, E., Rinaldo, L., and Hansel, C. (2011) SK2 channel expression and function in cerebellar Purkinje cells. *J. Physiol.*

p75 Regulates SK Channels in Purkinje Cells

589, 3433–3440

43. Schwartz, P. M., Borghesani, P. R., Levy, R. L., Pomeroy, S. L., and Segal, R. A. (1997) Abnormal cerebellar development and foliation in BDNF^{-/-} mice reveals a role for neurotrophins in CNS patterning. *Neuron* **19**, 269–281
44. Zagrebelsky, M., Holz, A., Dechant, G., Barde, Y. A., Bonhoeffer, T., and Korte, M. (2005) The p75 neurotrophin receptor negatively modulates dendrite complexity and spine density in hippocampal neurons. *J. Neurosci.* **25**, 9989–9999
45. Chapleau, C. A., and Pozzo-Miller, L. (2012) Divergent roles of p75NTR and Trk receptors in BDNF's effects on dendritic spine density and morphology. *Neural Plast.* **2012**, 578057–578059
46. Minichiello, L., Calella, A. M., Medina, D. L., Bonhoeffer, T., Klein, R., and Korte, M. (2002) Mechanism of TrkB-mediated hippocampal long-term potentiation. *Neuron* **36**, 121–137
47. He, X. P., Pan, E., Sciarretta, C., Minichiello, L., and McNamara, J. O. (2010) Disruption of TrkB-mediated phospholipase C γ signaling inhibits limbic epileptogenesis. *J. Neurosci.* **30**, 6188–6196
48. Li, Y., Jia, Y. C., Cui, K., Li, N., Zheng, Z. Y., Wang, Y. Z., and Yuan, X. B. (2005) Essential role of TRPC channels in the guidance of nerve growth cones by brain-derived neurotrophic factor. *Nature* **434**, 894–898
49. Lang, S. B., Stein, V., Bonhoeffer, T., and Lohmann, C. (2007) Endogenous brain-derived neurotrophic factor triggers fast calcium transients at synapses in developing dendrites. *J. Neurosci.* **27**, 1097–1105
50. Blum, R., Kafitz, K. W., and Konnerth, A. (2002) Neurotrophin-evoked depolarization requires the sodium channel Na_v1.9. *Nature* **419**, 687–693
51. Carter, A. R., Chen, C., Schwartz, P. M., and Segal, R. A. (2002) Brain-derived neurotrophic factor modulates cerebellar plasticity and synaptic ultrastructure. *J. Neurosci.* **22**, 1316–1327
52. Xu, Z. Q., Sun, Y., Li, H. Y., Lim, Y., Zhong, J. H., and Zhou, X. F. (2011) Endogenous proBDNF is a negative regulator of migration of cerebellar granule cells in neonatal mice. *Eur. J. Neurosci.* **33**, 1376–1384
53. Matsumoto, T., Rauskolb, S., Polack, M., Klose, J., Kolbeck, R., Korte, M., and Barde, Y. A. (2008) Biosynthesis and processing of endogenous BDNF: CNS neurons store and secrete BDNF, not pro-BDNF. *Nat. Neurosci.* **11**, 131–133
54. Yang, J., Siao, C. J., Nagappan, G., Marinic, T., Jing, D., McGrath, K., Chen, Z. Y., Mark, W., Tessarollo, L., Lee, F. S., Lu, B., and Hempstead, B. L. (2009) Neuronal release of proBDNF. *Nat. Neurosci.* **12**, 113–115
55. Borghesani, P. R., Peyrin, J. M., Klein, R., Rubin, J., Carter, A. R., Schwartz, P. M., Luster, A., Corfas, G., and Segal, R. A. (2002) BDNF stimulates migration of cerebellar granule cells. *Development* **129**, 1435–1442
56. Zhou, P., Porcionatto, M., Pilapil, M., Chen, Y., Choi, Y., Tolia, K. F., Bikoff, J. B., Hong, E. J., Greenberg, M. E., and Segal, R. A. (2007) Polarized signaling endosomes coordinate BDNF-induced chemotaxis of cerebellar precursors. *Neuron* **55**, 53–68
57. Storey, N. M., O'Bryan, J. P., and Armstrong, D. L. (2002) Rac and Rho mediate opposing hormonal regulation of the ether-a-go-go-related potassium channel. *Curr. Biol.* **12**, 27–33
58. Kinoshita, H., Matsuda, N., Kaba, H., Hatakeyama, N., Azma, T., Nakahata, K., Kuroda, Y., Tange, K., Iranami, H., and Hatano, Y. (2008) Roles of phosphatidylinositol 3-kinase-Akt and NADPH oxidase in adenosine 5'-triphosphate-sensitive K⁺ channel function impaired by high glucose in the human artery. *Hypertension* **52**, 507–513
59. Nolz, J. C., Gomez, T. S., Zhu, P., Li, S., Medeiros, R. B., Shimizu, Y., Burkhardt, J. K., Freedman, B. D., and Billadeau, D. D. (2006) The WAVE2 complex regulates actin cytoskeletal reorganization and CRAC-mediated calcium entry during T cell activation. *Curr. Biol.* **16**, 24–34
60. Beech, D. J. (2007) Canonical transient receptor potential 5. *Handb. Exp. Pharmacol.* **179**, 109–123
61. van der Wijst, J., Hoenderop, J. G., and Bindels, R. J. (2009) Epithelial Mg²⁺ channel TRPM6: insight into the molecular regulation. *Magnes. Res.* **22**, 127–132
62. Karpushev, A. V., Ilatovskaya, D. V., Pavlov, T. S., Negulyaev, Y. A., and Staruschenko, A. (2010) Intact cytoskeleton is required for small G protein dependent activation of the epithelial Na⁺ channel. *PLoS One* **5**, e8827
63. Liebau, S., Steinestel, J., Linta, L., Kleger, A., Storch, A., Schoen, M., Steinestel, K., Proepper, C., Bockmann, J., Schmeisser, M. J., and Boeckers, T. M. (2011) An SK3 channel/nWASP/Abi-1 complex is involved in early neurogenesis. *PLoS One* **6**, e18148
64. Takenawa, T., and Suetsugu, S. (2007) The WASP-WAVE protein network: connecting the membrane to the cytoskeleton. *Nat. Rev. Mol. Cell Biol.* **8**, 37–48
65. Padrick, S. B., and Rosen, M. K. (2010) Physical mechanisms of signal integration by WASP family proteins. *Annu. Rev. Biochem.* **79**, 707–735
66. Karpushev, A. V., Levchenko, V., Ilatovskaya, D. V., Pavlov, T. S., and Staruschenko, A. (2011) Novel role of Rac1/WAVE signaling mechanism in regulation of the epithelial Na⁺ channel. *Hypertension* **57**, 996–1002
67. Kim, Y., Sung, J. Y., Ceglia, I., Lee, K. W., Ahn, J. H., Halford, J. M., Kim, A. M., Kwak, S. P., Park, J. B., Ho Ryu, S., Schenck, A., Bardoni, B., Scott, J. D., Nairn, A. C., and Greengard, P. (2006) Phosphorylation of WAVE1 regulates actin polymerization and dendritic spine morphology. *Nature* **442**, 814–817
68. Ito, M. (1984) *The Cerebellum and Neural Control*, Raven, New York
69. Raman, I. M., and Bean, B. P. (1999) Ionic currents underlying spontaneous action potentials in isolated cerebellar Purkinje neurons. *J. Neurosci.* **19**, 1663–1674
70. Walter, J. T., Alviña, K., Womack, M. D., Chevez, C., and Khodakhah, K. (2006) Decreases in the precision of Purkinje cell pacemaking cause cerebellar dysfunction and ataxia. *Nat. Neurosci.* **9**, 389–397